Effects of Ga doping on the structural, optical and electronic properties of PbS:

Experimental and computational study

By

Kelemu Teshome Assefa

A THESIS SUBMITTED TO

GRADUATE PROGRAM OF

ADDIS ABABA UNIVERSITY

IN PARTIAL FULFILLMENT OF THE REQUIREMENTS

FOR THE DEGREE OF

MASTERS OF SCIENCE IN PHYSICS

(CONDENSED MATER PHYSICS)

ADDIS ABABA, ETHIOPIA

OCTOBER 2021

© Copyright by Kelemu Teshome Assefa, 2021

ADDIS ABABA UNIVERSITY

PROGRAM OF GRADUATE STUDIES

Effects of Ga doping on the structural, optical and electronic properties of PbS:

Experimental and computational study

By

Kelemu Teshome Assefa

Department of physics

Addis Ababa University

Approved by the Examining Board

Chairman: ______________________________
Signature

External Examiner: ______________________________
Signature

Internal Examiner: ______________________________
Signature

Advisor: ______________________________-
Signature

Date: October 2021

ADDIS ABABA UNIVERSITY

Date: October 2021

Author: **Kelemu Teshome Assefa**

Title: **Effects of Ga doping on the structural, optical and electronic properties of PbS: Experimental and computational study**

Department: **Department of Physics**

Degree**: M.Sc** Convocation: **October** Year: 2021

Permission is here with granted to Addis Ababa university to circulate and to have copied for non-commercia; purposes, at its discretion, the above title upon the request of individuals or institution

____

Signature of Author

THE AUTHOR RESERVES OTHER PUBLICATION RIGHTS AND NEITHER THE THESIS NOR EXTENSIVE EXTRACTS FROM IT MAY BE PRINTED OR OTHERWISE REPRODUCED WITHOUT THE AUTHOR'S WRITTEN PERMISSION

THE AUTHOR OF A THESIS THAT PERMISSION HAS BEEN OBTAINED FOR THE USE OF ANY COPYRIGHTED MATERIAL APPEARING IN THIS THESIS (OTHER THAN BRIEF EXCERPTS REQUIRING ONLY PROPER ACKNOWLEDGEMENT IN SCHOLARLY WRITING) AND THAT ALL SUCH USE IS CLEARLY ACKNOWLEDGED.

This Work is Dedicated

to My parents

Acknowledgements

I would like to express my deep gratitude to my research advisors Dr. Fekadu Gashaw and Dr Mesfin Birile, for their unlimited advice on planning and development of this research work and assistance in keeping my progress on schedule, patient guidance, enthusiastic encouragement and useful critiques of this research work. Again, I would like to appreciate them for their politeness approach without filling their stateless.

I would also like to extend my thanks to Addis Ababa University, Department of Physics Instructors and staff members also the other bodies that I want to address my deep thank for their limitless support and encouragement the technicians of the laboratory of the physics department for their help in offering me the resources in running the program.

Finally, I wish to thank my parents for their support and encouragement throughout my study.

ALL PRAISE IS DUE TO ALLAH ALONE!!!

Table of Contents

Dedication. i
Acknowledgements ii
Table of Contents iii
List of Table v
List of Figures vi
Abbreviations viii
Symbols x
Abstract xi

1. GENERAL INTRODUCTION 1

1.1. Semiconductors 1
1.2. Applications of Semiconductors 6
1.3. Thin film and Semiconductors 8
1.4. General properties of Lead Sulfide 9
1.5. Statement of the problem 9
1.6. Objective of the Study 10
1.6.1. General objectives of the Study 10
1.6.2. Specific objectives of the Study 10
1.7. Significance of the study 11

2. LITERATUREREVIEWS **12**

2.1. Experimental works 12
2.2. Computational works 13

3. METHODOLOGY **15**

3.1. Experimental 15
3.1.1. Thin films deposition techniques 15

3.1.2. Basics of CBD. 16
3.1.3. Effects of Bath Temperature and Deposition Time 17
3.1.4. Thin film characterization 19
3.2. Computational 20
3.2.1. Basics of DFT 20
3.2.2. Practical Implementation 27
3.2.3. Quantum Espresso 29
3.3. Experimental Procedures and Computational Details 30
3.3.1. Experimental procedures 30
3.3.2. Computational Details 31

4. RESULTS AND DISCUSSIONS **32**

4.1. Experimental Results 32
4.1.1. Structural Analysis 32
4.1.2. Optical Analysis 37
4.1.3. PL Study 40
4.2. Computational Results 42
4.2.1. Structural Properties.. 43
4.2.2. Electronic Property..45

5. CONCLUSION **56**

References **57**

Appendixes **61**

List of Tables

1.1.General properties of Lead Sulfide 9

4.1 X-ray diffraction parameters of the undoped and Ga- doped
Pbs films from the (111) orientation ………………………………………… …. 35

4.2 X-ray diffraction parameters of the undoped and Ga- doped
Pbs films from the (200) orientation. ………………………………………… 36

4.3 Calculated optical band gap of undoped PbS and Ga doped PbS. ………………… .39

4.4 Results of lattice parameters of PbS, $Ga_1Pb_7S_8$, $Ga_1Pb_7S_8$ $Ga_1Pb_7S_8$
with theoretical experimental, and other DFT calculations. ………………………. 45

4.5 Performance of PBE and PBEsol functionals on band gap calculation……………. 47

4.6 Effects of Super cell on the band gap. …………………………………………….. 48

4.7 Effects of Ga-doping on lattice parameter and energy band gap of PbS. …………. 48

4.8 Results of electronic band gap of PbS, $Ga_1Pb_7S_8$, $Ga_2Pb_6S_8$,
$Ga_3Pb_5S_8$ and $Ga_4Pb_4S_8$ with theoretical, experimental, and other
DFT calculations. …………………….. ……………………………………48

List of Figures

1.1.Energy diagrams for insulators, semiconductors, and conductors. 1
1.2. Bohr diagrams of the silicon and copper atoms. …………………………………… 2
1.3. Intrinsic Semiconductor. ……………………………………………………………..3
1.4. Covalent bonds in a silicon crystal. …………………………………………………4
1.5. n-type and p type semiconductors. ………………………………………………… 6
4.1.The XRD pattern of PbS and Ga doped PbS thin films for
different Ga concentration………………………………………………………......33
4.2.Extended X-ray diffraction patterns of the A. (111) and B.
the (200) plane peaks for pure and Ga doped PbS thin films...……………………...... 33
4.3. $(\alpha h\nu)^2$ vs photoenergy $(h\nu)$ of undoped and Ga-doped PbS………………………38
4.4.Photoluminescence emission spectrum of pure and Ga doped PbS thin films ……...41
4.5.Detail view for Photoluminescence emission spectrum of:
(a) Ga % of (2,6 and 15), (b) Ga % of (0, 4 and10) and (c) Ga 8% thin film. ……. 41
4.6.Optimized lattice strutueres of (a) pure PbS (b) Pb_8S_8 (c) $Ga_1Pb_7S_8$
(d), $Ga_2Pb_6S_8$, (e) $Ga_3Pb_5S_8$,and (f) $Ga_4Pb_4S_8$……………………………………43
4.7.Total energy as afubction of lattice constant pure PbS with (a) PBEsol
(b) PBE functional (c) $Ga_1Pb_7S_8$ (d), $Ga_2Pb_6S_8$,
(e) $Ga_3Pb_5S_8$,and (f) $Ga_4Pb_4S_8$ ……………………………………………………...44
4.8.Electronic band structures of PbS (a) with Fermi level
(b) Normalized (Fermi level set to 0) (c) Pb_8S_8. …………………………………...46
4.9.Electronic band structure of (a) $Ga_1Pb_7S_8$
(b)$Ga_2Pb_6S_8$, (c) $Ga_3Pb_5S_8$,and (d) $Ga_4Pb_4S_8$ calculated by
PBEsol XC functional ……………………………………………………………….49
4.10. Electronic band structure of (a) $Ga_1Pb_7S_8$ (b)$Ga_2Pb_6S_8$,
(c) $Ga_3Pb_5S_8$,and (d) $Ga_4Pb_4S_8$ calculated by PBE functional. ………………… 50
4.11. DOS of (a) PbS and (b) Pb_8S_8 …..…………………………………………….. 52
4.12. DOS of $Ga_1Pb_7S_8$ ...…………………………………………………… 53

4.13. DOS of $Ga_2Pb_6S_8$ ………………………………………………………………… 54
4.14. DOS of $Ga_3Pb_5S_8$ …………………………………………………………………54
4.15. DOS of $Ga_4Pb_4S_8$ ……………………………………… ……… ……………… 55

Abbreviations

LED = Light Emission Diode
DFT = Density functional theory
XRD = X-Ray Diffraction
PVD = physical vapor deposition
CVD = Chemical vapor deposition
ALE = Atomic Layer Epitaxy
CD = Chemical Deposition
FET = Fringes of equal thickness
FECO = Fringes of equal chromatic order
SEM = Scanning Electron Microscopy
TEM = Transmission Electron Microscopy
EDX = Energy-dispersive analysis
AES = auger electron spectroscopy
XPS = X-say photoelectron spectroscopy
HEG = homogeneous electron gas
FP-LAPW = Full potential linearized augmented plane wave
PW = Plane wave
LDA = The Local Density Approximation
GGA = Generalized gradient approximation
BZ = Brillouin zone
QE = Quantum-ESPRESSO
XC = Exchange-correlation
PBE = Perdew-Burke-Ernzerhof
PBEsol = Perdew-Burke-Ernzerhof for solid
PP = Pseudopotentials
UV–Vis = Ultra-Violet visible
PL = Photoluminescence

VESTA = visualization for electronic and structural analysis

FCC = Face centered cubic

DOS = Density of State

VB = Valence band

CB = Conduction band

Symbols

H = Hamiltonian

Ψ = wave-function

K_{sp} = Solubility product

Z = atomic number

n = electron density

E_0 = ground-state energy

$\hbar$ = Reduced Planck's constant

v_{eff} = Effective potential

$\vec{k}$ = wave vector

a = lattice parameter,

D = crystalline size

λ = wavelength

h = Planck's constant

E_g = Energy gap

α = Absorption coefficient

ε = Strain

δ = Dislocation density

Abstract

Experimental and computational methods were employed to study the effects of Ga doping on the structural electronic and optical properties of Pbs. Chemical bath deposition method was used to prepare pure and Ga doped PbS thin films at a bath temperature of 80^0C and a pH of 11. The XRD results confirmed that the prepared Ga doped and undoped PbS had a face center crystal structure with a preferential orientation along the (111) plane. The experimental results further revealed that Ga doping had considerable effect on the structural parameters and optical band gap of PbS. In addition, the photoluminescence study verified the material luminescence intensity is dependent on the crystalline size. Density functional theory (DFT) calculations were also performed to study the effect of Ga doping based on General Gradient Approximation. The performance of Perdew-Burke-Ernzerhof (PBE) and bulk solids (PBEsol) exchange-correlation functionals were tested. The lattice constant of pure PbS calculated by PBE and PBEsol functionals were found to be 6.0 Å and 5.913 Å, respectively, while its calculated energy band gap was found to be 0.498 eV for PBE and 0.392 eV for PBEsol. Band structure calculations with PBEsol revealed that PbS is direct band gap semiconductor with its Fermi level lying exactly in between 8.214 eV and 7.822 eV. The incorporations of Ga impurity on PbS molecule were studied systematically with the concentration percentage of 12.5 %, 25 %, 37.5 % and 50 %. We found that the lattice parameters of Ga doped PbS decreased from 5.913 Å to 5.795 Å while, the band gap increased from 0.0354 eV to 0.2579 eV and 0.0411eV to 0.2603 eV calculated by PBEsol and PBE respectively. All the experimental and computational studies verified that Ga doping had a significant effect on the structural and electronic properties of PbS.

CHAPTER 1

General Introduction

1.1. Semiconductors

Semiconductors are defined by their unique electric conductive behavior, somewhere between that of a conductor and an insulator [1]. Semiconductors constitute a large class of substances which have resistivities lying between those of insulators and conductors. *i.e.*, lying in the range **10^{-4} to 10^{4} Ω-m**.

The elemental materials, those that are composed of single species of atoms include silicon and germanium. Silicon is by far the most common semiconductor used in integrated circuits and will be emphasized to a great extent [2].

Energy band

The difference in energy between the valence band and the conduction band is called an energy gap or **band gap.**

This is the amount of energy that a valence electron must gain in order to jump from the highest valence band energy to the lowest energy in conduction band. Once in the conduction band the electron is free to move throughout the material and is not tied to any given atom.

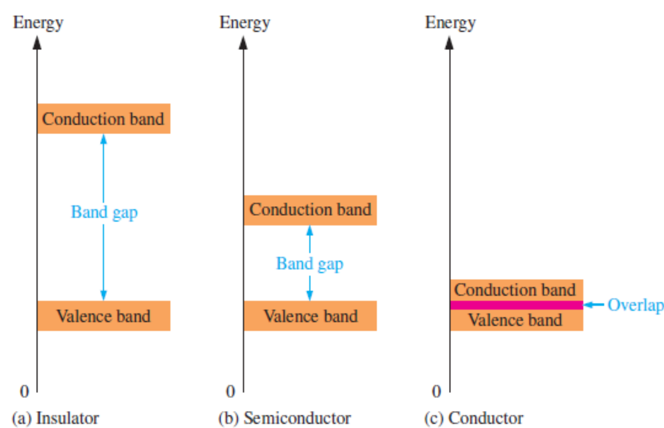

Fig.1.1: Energy diagrams for insulators, semiconductors, and conductors.

The energy gap or band gap is the difference between two energy levels and electrons are "not allowed" in this energy gap based on quantum theory [3]. Although an electron may not exist in this region, it can "jump" across it under certain conditions [4]. For insulators, the gap can be crossed only when breakdown conditions occur—as when a very high voltage is applied across the material.

The band gap is illustrated in Figure 1.1(a) for insulators. In semiconductors the band gap is smaller, allowing an electron in the valence band to jump into the conduction band if it absorbs photon energy equivalent to E_g . The band gap depends on the semiconductor material. This is illustrated in Figure 1.1(b). In conductors, the conduction band and valence band overlap, so there is no gap, as shown in Figure 1.1(c). This means that electrons in the valence band move freely into the conduction band, so there are always free electrons rotating the lattice

Comparison of a Semiconductor Atom to a Conductor Atom

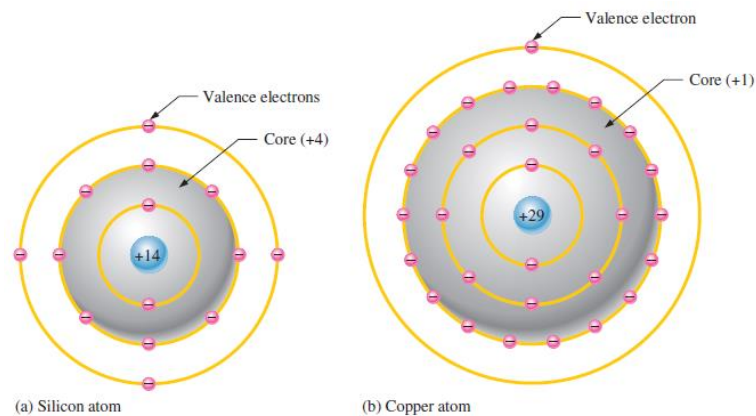

Figure 1.2: Bohr diagrams of the silicon and copper atoms

Silicon is a semiconductor and copper is a conductor. Bohr diagrams of the silicon atom and the copper atom are shown in Figure 1,2. Notice that the core of the silicon atom has a net charge of +4 (14 protons – 10 electrons) and the core of the copper atom has a net

charge of +1(29 protons – 28 electrons). Recall that the core includes everything except the valence electrons.

The valence electron in the copper atom "feels" an attractive force of +1 compared to a valence electron in the silicon atom which "feels" an attractive force of +4. Therefore, there is more force trying to hold a valence electron to the atom in silicon than in copper. The copper's valence electron is in the fourth shell, which is a greater distance from its nucleus than the silicon's valence electron in the third shell. Recall that, electrons farthest from the nucleus have the most energy. The valence electron in copper has more energy than the valence electron in silicon. This means that it is easier for valence electrons in copper to acquire enough additional energy to escape from their atoms and become free electrons than it is in silicon. In fact, large numbers of valence electrons in copper already have sufficient energy to be free electrons at normal room temperature

Covalent Bonds

Figure 1.3 shows how each silicon atom positions itself with four adjacent silicon atoms to form a silicon crystal, which is a three-dimensional symmetrical arrangement of atoms. A silicon (Si) atom with its four valence electrons shares an electron with each of its four neighbors. This effectively creates eight shared valence electrons for each atom and produces a state of chemical stability. Also, this sharing of valence electrons produces a strong **covalent bond** that hold the atoms together; each valence electron is attracted equally by the two adjacent atoms which share it. Covalent bonding in an intrinsic silicon crystal is shown in Figure 1.4. An **intrinsic** crystal is one that has no impurities. Covalent bonding for germanium is similar because it also has four valence electrons.

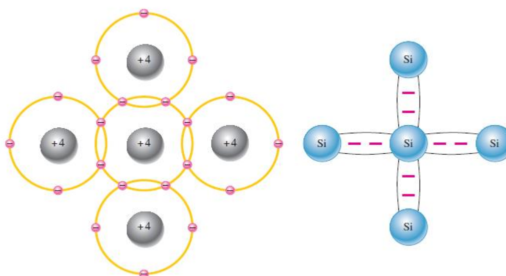

Figure 1.3: Intrinsic Semiconductor, (a)The center silicon atom shares an electron with each of the four surrounding silicon atoms, creating a covalent bond with each. The surrounding atoms are in turn bonded to other atoms, and so on. (b) Bonding diagram. The red negative signs represent the shared valence electrons

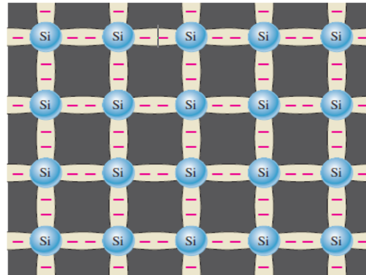

Figure 1.4: Covalent bonds in a silicon crystal

Semiconductors Classification

Two general classifications of semiconductors are, **the elemental semiconductor materials**: found in group IV of the periodic table, and **the compound semiconductor materials**: most of which are formed from special combinations of group III and group V elements.[2]

Elemental Semiconductors are broadly classified in to two

- Intrinsic (pure)
- Extrinsic(doped)

Intrinsic semiconductors

semiconductor material for which gap between valence band and conduction band is small; (gap width in Si is 1.1 eV, in Ge 0.7 eV).at T = 0, there are no electrons in the conduction band,
and the semiconductor does not conduct (lack of free charge carriers);
at T > 0, some fraction of electrons has sufficient thermal kinetic energy to overcome the gap and jump to the conduction band

A silicon crystal is different from an insulator because at any temperature above absolute zero temperature, there is a finite probability that an electron in the lattice will be knocked loose from its position, leaving behind an electron deficiency called a "hole".

This hole can travel from one atom to the adjacent atom by accepting an electron from later one.
This process involves formation of new covalent bond and breaking an existing bond by filling up the hole and creating a new hole.in this way, the holes travel from one atom to the adjacent atoms in crystal lattice.

Extrinsic Materials

The characteristics of semiconductor materials can be altered significantly by the addition of certain impurity atoms into the relatively pure semiconductor material. Semiconductor material that has been subjected to the doping process is called extrinsic material. Doping of 1 part impurity in 10 billion is sufficient. N and P type materials are formed by adding a predetermined number of impurity atoms into a Ge or Si base.

P Type Material: By doping a pure Si crystal with group III trivalent impurities such as Boron (B), Gallium (Ga) and Iridium (Id), p-type materials are formed. There is now an insufficient number of electrons to complete the covalent bonds of the newly formed lattice. The resulting vacancy is called a hole (+). The vacancy accepts a free electron. So, the trivalent diffused impurities are called acceptor atoms. P-type is also electrically neutral**. N Type Material:** By introducing group V pentavalent impurities such as antimony (Sb), Arsenic (As) and Phosphorus (P). Fifth electron unassociated with any particular covalent bond loosely bond to its parent atoms (Sb) is relatively free to wave within the newly formed n-type material. Semiconductor shows reduction in resistance. The inserted impurity atom has denoted a relatively “free” electron to the structure. So diffused impurities with five valence electrons are called donor atoms. N-type materials are electrically neutral. Donor level makes the energy gap smaller. Due to the lower energy gap, a large number of electrons are available in the conduction band at room temperature

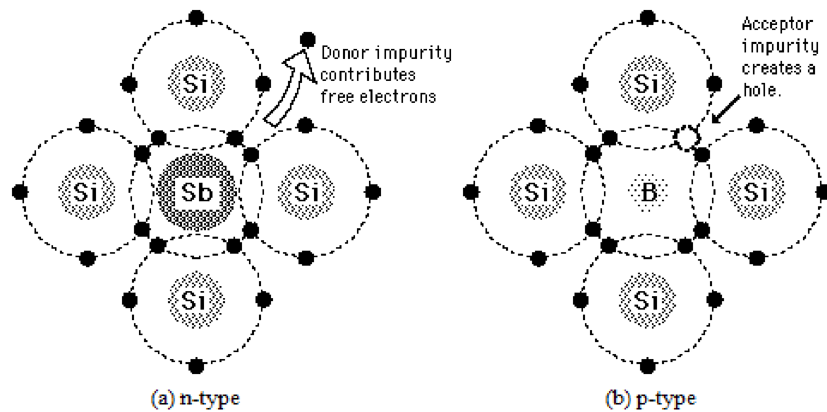

Figure 1.5: n-type and p type semiconductors

Compound semiconductor materials

A compound semiconductor is a semiconductor compound composed of chemical elements of at least two different species. These semiconductors Compound semiconductors typically form in periodic table groups (group III–V), for example of elements from the Boron group boron, aluminum, gallium, indium) and from group V, nitrogen, phosphorus, arsenic, antimony, bismuth). The range of possible formulae is quite broad because these elements can form binary (two elements, e.g. gallium (III) arsenide (GaAs)), ternary (three elements, e.g. indium gallium arsenide (InGaAs)) and quaternary (four elements, e.g. aluminum gallium indium phosphide (AlInGaP)) alloys.

1.2. Applications of Semiconductors

Today semiconductor devices are omnipresent in a wide range of industries, including computers, communications, aerospace, manufacturing, agriculture, and healthcare. some their properties in those sectors revised as:[5].

Electronic Devices

Semiconductors have made electronic devices – such as MP3 players, HDTVs / TVs, CD players, computers, and cell phones –smaller, cheaper, faster, and more reliable. Science and industry also depend heavily on semiconductor devices. Research laboratories use these devices in all sorts of electronic instruments to perform tests, measurements, and numerous other experimental tasks.

Industrial control systems (such as those used to manufacture automobiles) and automatic telephone exchanges also use semiconductors. Even today heavy-duty versions of the solid-state rectifier diode are being use to convert large amounts of power for electric railroads. Of the many different applications for solid-state devices, space systems, computers, and data processing equipment are some of the largest consumers.

Solar Cells

Now-a-days most of the solar cells the absorption of photons, as a result of the generation of the charge carriers, and the subsequent separation of the photo-generated charge carriers take place in semiconductor materials. Therefore, the semiconductor layers are the most important parts of a solar cell and they form the central part of the solar cell. There are a number of different semiconductor materials that are suitable for the conversion of photons energy into electrical energy. The crystalline silicon (c-Si) solar cell, which dominates the PV market at present, has a simple structure, and provides a superior example of a typical solar cell structure.[5]

Transmitters and Receivers

Optical communication literally begins and ends with a transmitter and receiver. In the transmitter, lasers produce light to travel down the fiber encoded with information. In the end, the receiver converts this light to an electronic signal via a photodiode detector. Thin alloy semiconductor films play an important role in both components.

In Computers

Semiconductors are one of the most important enabling technologies for digital computers. They are the foundation of all modern electronic devices which use circuitry. These materials were first introduced to computing to solve issues related to vacuum tubes used in analog computers. The tubes would often leak, and the metals used to transmit electrons within them would frequently burn out. Semiconductors did not suffer these issues. Semiconductor materials conduct electrons in an entirely different manner than metals, causing them to avoid burn out. Unlike vacuum tubes, semiconductors did not need to warm up over long periods of time prior to use. Additionally, they required far less space than a series of vacuum tubes. The first semiconductor-based transistor was made in 1947. The first integrated circuit based on semiconductor technology followed shortly after, in 1959. All the semiconductor materials are not used in computers. The material which has become the standard semiconductor for circuitry is silicon. Silicon is the most abundant element in the earth's crust, and is accessible from almost anywhere on earth. This makes silicon inexpensive, driving down the cost of computers and other technological devices. Some computers use other semiconductor materials to achieve faster electron conduction speeds. An example is germanium with a small concentration of arsenic impurities. While this material achieves faster conduction rates, its cost is significantly higher than silicon.

1.3. Thin Film and Semiconductors

A **thin film** is a layer of material ranging from fractions of a nanometer (monolayer) to several micrometers in thickness. the controlled synthesis of materials as thin films (a process referred to as deposition) is a fundamental step in many applications. The expressions "Thin films" and "Semiconductor technology" are almost synonyms. It is true, there is some semiconductor technology that does not need thin films but not much comes to mind right away. There is, however, quite a bit of thin film technology outside of semiconductor technology, e.g., in **optics**. In fact, so in our days we have semiconductors in the form of nano crystals or (thin film). examples of thin film semiconductors are

Cadmium oxide (Cdo), lead Oxide (Pbo), Sulfides of Cadmium, Lead and Copper (Lead sulphide (Pbs).

1.4. General properties of Lead sulfide

Lead (II) sulfide (also spelled *sulphide*) is an inorganic compound with chemical formula PbS. **Galena** is the principal ore and the most important compound of lead. At normal temperature and pressure Lead sulfide (PbS) rock-salt structure is a narrow band gap semiconductor material. Lead sulfide is an important IV-VI group semiconductor, which has attracted much attention because of its special small direct-band gap (0.41 eV) and large excitonic Bohr radius of 18 nm. PbS large size effects of quantization because of the small "effective mass" of electron and holes and the large dielectric constant.

Table 1.1: General properties of Lead Sulfide

Electrical		**Magnetic**		**Optical**	
Band Gap	0.41 eV	Magnetic Susceptibility	- 0.0000836	Refractive Index	3.91
Electron/Hole Mobility	600 cm2/Vs				
Electric Susceptibility (χc)	4.808 at λ =1000 nm				

1.5. Statement of the problem

Thanks to semiconductors they make our life easy. Almost all todays technological products in any sector are a result of semiconductors electronics, health, agriculture, space technology, telecommunication, Industries, Aviation, energy and more.

The recent and more attractive area of research is Nano-technologies, one of them is Thin film semiconductor. thin film has an advantage because of its size, low energy consumption cost-effective, easy for production, product material availability, and so on

Semiconductors have low and limited operational voltage, are electrostatic sensitive devices (ESDS) must release with appropriate operational manuals also caution and warning in order to give aware of personals. The properties that semiconductors have depends up on the area in which we are going to use them All this must be filled before we use them.

Lead Sulfide is one of narrow band gap semiconductor thin film and has applications in many fields such as solar cells, solar absorbers, photographs, lasers, LED devices, telecommunications, detectors, optical switches, optical amplification, and also a gas-sensing agent in the solid- state sensors. So that is the fact that takes advantage over large band gap semiconductors, this work will have contribution in the related areas of computational and experimental works

1.6. Objectives of the Study

1.6.1. General objective

The objective of this research is to study the effects of Ga doping on the structural, electronic and optical properties of Lead Sulfide (Pbs) experimentally and computationally.

1.6.2. Specific objectives

- Optimize the deposition condition of undoped and Ga doped PbS from Hexamethylenediamine complexing agent.
- Synthesize both undoped and Ga doped PbS by using chemical bath deposition (CBD) method.

- Study the influence of Ga doping on the structural and electronic properties of PbS experimentally.
- Study structural and electronic properties of Ga doped and undoped PbS Computationally with DFT basis.
- Compare and verify the experimental works with DFT results.

1.7. Significance of the Study

Properties of thin film semiconductors are absolutely dependent up on their structure. In other word, it means that a change in their structure cause an alteration on their optical, morphological, electrical and optoelectronic properties. Therefore, studding the properties of semiconductors for both computationally and experimentally is vital to understand the correlation between their structures and their properties. Computational studies have advantages over the real experiments because one can model any material easily without restriction and study the various properties by based on the information about their structure and composition. The main goal of this research to have a significant contribution to computational and experimental works on study of bulk PbS and the effect of Ga-doping on structural, electronic and optical properties of PbS.

CHAPTER 2
Literature Reviews

2.1. Experimental Works

Various experimental results show that the inclusions of impurity atoms in PbS lattice may changes its electronic structure which also alter its optical, morphological and optoelectronic properties. S. Sankar et al. studied Mg doping effects on the physical properties of lead sulfide thin films. The film synthesized by using the chemical bath deposition technique with deposited at 300°C for 2 hours. The results reveal the films have polycrystalline nature with uniform and smooth surface, the average crystallite size is found to be in the range between 20.03 and 15.12 nm. Also, from their optical studies energy band gap of the thin film increase from 1.54 to 1.66 eV with increasing Mg doping concentration [6]. Chidambara Kumar et al performed structural, optical and magnetic studies of Mn doped PbS thin films by successive ionic layer adsorption and reaction deposition method. (SILAR) method. According to their results, Mn doped Pbs thin films ware polycrystalline in nature with preferential orientation along (200) plane and uniform surface. The bandgap energy of PbS and Mn doped PbS thin films were 2.4 eV and 3.1 eV additionally their study reveals that the thin film exhibit multi domain behavior [7]. Another study carried out by Reshmi Radhakrishnan in et al, effect of Ga doping on the physical properties of lead sulfide thin films, in the study the photo sensitivity measurements result indicates the suitability of the doped films for photovoltaic applications due to the blue shift in the band gap to 2.37 eV [11]. moreover, Y. Gülen et al studied characteristics of Ba-doped Pbs thin films Prepared by the SILAR Method as the scanning electron microscopy analysis indicates the Ba-doping concentration influences the size of the thin film, XRD result shows all the films are in face centered cubic structure more over their optical study shows optical band gap of the film increases as Ba-doping concentration is increased [9]. M. G. Faraj et al studied structural, morphological and electrical properties of Zn doped PbS thin film, the film synthesized by chemical spray pyrolysis technique. The study result indicates the film grain size and surface roughness decreases with increasing Zn concentration. Additionally, their electrical study with at 1, 2

and 3 % Zn dopants concentrations indicate that the film coated with at 3 % Zn dopant has a maximum carrier concentration of $1.39 \times 10^{10} cm^{-3}$ due to this they found that the film coated with 3 % Zn dopant has better structural, morphological and electrical properties [10]. Recently Jiabin Huo et al studied Effect of Cr Doping Concentration on the Structural, optical, and Electrical Properties of Lead Sulfide (PbS) Nanofilms, the result reveals that the variation in Cr concentration led to different grain shapes, and the grain size became smaller with the increasing doping concentrations. According to the optical study 2 at. % Cr-doped PbS nanofilms exhibited the best optical and electrical properties, suitable for solar cell applications [8].

2.2. Computational Works

Computational studies are available for doped and undoped group II-VI compound semiconductors. For instant, Hai-Qing Xie et al used the first principal plane-wave pseudo potential method to investigate on the electronic and optical properties of ZnS with and without La-dopant. Their results revealed that La-doping narrows the band gap of ZnS systems and La doped ZnS system changes from semiconductor into metal through the Mott transition [12]. Heidi D. Nelson et al investigated the electronic structures of copper-doped CdSe nanocrystals by using time-dependent density functional theory. The obtained results yield fundamental insights into the electronic structures and photophysical properties of copper-doped semiconductor NCs relevant to their potential applications [13]. M. Junaid Iqbal Khan et al. applied a computational approach focused on optical properties of Ni-doped rock salt CdS system under PBE-GGA and GGA + U approximations. The study of optical properties of CdS:Ni system carried out by fixing super cell size and increasing dopant concentration and they found that Ni-doping in CdS host lattice enhances its opto-electronic properties [14]. The same research group M. Junaid Iqbal Khan et al used DFT study to predict optical and electronic properties of Na doped CdS system. The entire study has been executed using Wien2k code by employing PBE-GGA approximation. Cd atoms were substituted with Na atoms and a change in optical properties is studied while size of super cell (1x2x2) is kept constant for all cases. They reported that the TDOS and PDOS illustrate dominant role of S atoms (p-orbital) while contribution of Cd d-states and dopant (Na) p-states. Moreover, optical absorption shows blue shift as Na

concentration was increased [15]. Asghar Khan M et al studied the structural, electronic and chemical bonding of the Sn doped PbX (X=S, Se, Te) materials by full potential linearized augmented plane wave method (FP-LAPW) within density functional theory (DFT). They found that the structural parameters varied with respect to doping [50]. First-principles electronic structure calculation applied by Zhong-Zhen Luo et al to study the thermoelectric performance of Ga-doped and Ga-In-co-doped n-type PbS. Their founding showed that Ga doping can cause Fermi level pinning in PbS by introducing a gap state between the conduction and valence band. Moreover, Ga addition significantly enhances the carrier concentration, electrical conductivity and power factor [51].

Literature survey revealed that only few reports are available on the computational studies of doped and undoped Group IV-VI semiconductors especially on PbS. This motivated to do this research. for the first time in this work hexamethylenediamine is being used as a complexing agent to deposit Ga doped and undoped PbS thin films. Furthermore, for the first time, we are reporting the influence of Ga doping on the structural, optical and electronic properties of PbS both computationally and experimentally. We optimized our computations using PBE and PBEsol functionals and the obtained results are in a good agreement with the experimental findings

CHAPTER 3

Methodology

3.1 Experimental

3.1.1 Thin films deposition techniques

Film deposition can be divided into two groups based on the nature of the deposition process. The physical methods include physical vapor deposition (PVD), laser ablation, molecular beam epitaxy, and sputtering. The chemical methods comprise gas phase deposition methods and solution techniques. The gas phase methods are chemical vapor deposition (CVD) [1, 2] and atomic layer epitaxy (ALE) [3], while spray pyrolysis [4], sol-gel [5], spin- [6] and dip-coating [7] and chemical bath deposition (CBD) [9] methods employ precursor solutions.

In general, Thin-film growth exhibits the following features:

- The birth of thin films of all materials created by any deposition technique starts with a random nucleation process followed by nucleation and growth stages.
- Nucleation and growth stages are dependent upon various deposition conditions, such as growth temperature, growth rate, and substrate chemistry.
- The nucleation stage can be modified significantly by external agencies, such as electron or ion bombardment.
- Film microstructure, associated defect structure, and film stress depend on the deposition conditions at the nucleation stage.
- The crystal phase and the orientation of the films are governed by the deposition conditions.

The basic properties of film, such as film composition, crystal phase and orientation, film thickness, and microstructure, are controlled by the deposition conditions. Thin films exhibit unique properties that cannot be observed in bulk materials:

- Unique material properties resulting from the atomic growth process.
- Size effects, including quantum size effects, characterized by the thickness, crystalline orientation, and multilayer aspects.

The properties of thin films are governed by the deposition method.

3.1.2. Basics of CBD

A. Solubility

A central concept necessary to understanding the mechanisms of CBD is that of the solubility product (K_{sp})[8]. The solubility product gives the solubility of a sparingly soluble ionic salt. K_{sp}, the product of the concentrations of the dissolved ions in general form for dissolution

$$M_aX_b \rightleftarrows aM^{n+} + bX^{m-} \quad \text{……………………………………… (3.1)}$$

Expressed as,

$$K_{sp} = [M^{n+}]^a[X^{m-}]^b \quad \text{……………………………………… (3.2)}$$

$[M^{n+}]^a[X^{m-}]^b$ is called the ionic product. The solubility product (K_{sp}) highly depends up on temperature since almost all CB**D** reactions are carried out in aqueous solutions, the pH of the deposition solution will give the concentration of OH^- ions in the solution. This pH is translated OH concentration, with in the very temperature-dependent ionization constant of water.

When the solution is saturated, the ionic product is equal to the solubility product. But when the ionic product exceeds the solubility product the solution is supersaturated precipitation occurs and ions combine on the substrate and in the solution to form nuclei. The more soluble is the salt, the greater the ion product and the greater is K_{sp}. However, K_{sp} also depends on the number of ions involved.

B. Complexation

Most chemical deposition (CD) reactions are carried out in alkaline solution. To prevent precipitation of metal hydroxides, a complexing agent (often called a ligand, since complexing agents to cations are electron donors) is added. The complex ant also reduces the concentration of free metal ions, which helps to prevent rapid bulk precipitation of the desired product. Ammonia is common complexing agent, by adding some amount of ammonia in the alkaline solution we can control the rate of precipitation of metal hydroxide the amount of ammonia to be added can be determined by calculating the stability constant between ammonia and soluble material.

C. Nucleation and Growth

Film formation occurs, whether deposition proceeds by ion-by-ion growth on the substrate (heterogeneous reaction) or by adsorption and coagulation of colloids that were formed in the solution (homogeneous reaction) [9].

Once (stable) nuclei have formed, there are several ways in which they can increase in size. One is a continuation of the process of embryo growth: absorption of ionic species from the solution onto the nucleus, growth of this type can be considered a self-assembling process. Another mechanism for crystal growth is known as Ostwald ripening. If a small nucleus or embryo is close to a larger crystal, the ions formed by (partial) dissolution of the smaller, less stable crystal can be incorporated into the larger crystal. As the smaller crystal becomes even smaller, its dissolution will become ever more favorable and eventually it will disappear. The result is that the larger crystals grow at the expense of the smaller ones. [9]

3.1.3. Effects of Bath Temperature and Deposition Time

As temperature increases dissociation of the complex increases hence the kinetic energy of the molecules also increases leading to greater interaction between ions and subsequent deposition at volume nucleation centers of the substrate [10]. This will result in increase or decrease of terminal thickness, depending on the extent of super saturation of the solution of the bath.

Experimentally, Srinivasan and Rajesh studied the effect of temperature on the structural and optical properties of PbS thin films [11] according to their result the crystallinity of films were improved when the temperature was increased from 30^0C to 60^0C with the preferred orientation growth along the (200) plane and the band gap energy decreases linearly from 1.2 eV to 0.9 eV

Effect of bath temperature on the chemical deposition of PbSe were studied by Anuar Kassim 2010 [16], their experiment caried out at bath temperatures 40, 60 and 80 °C. the results show the optimum bath temperature was 80, as the band gap energy decreased from 2.0 to 1.3 eV in contrast with bath temperature was increased from 40 to 80 °C. and the films deposited at 80 °C showed good crystallinity and uniformly distributed over the surface of substrate with larger grain sizes.

Effect of deposition temperature on the structural, morphological and optical band gap of chemically deposited PbSe thin films were studied by F. G. Hone and F. K. Ampong [17]. The samples were deposited at the bath temperatures of 60, 75 and 90^0C. The films deposited at higher temperatures exhibited sharp and intense diffraction peaks, indicating an improvement in crystallinity. The deposition temperature also had a strong influence on the preferred orientation of the crystallites as well as other structural parameters such as macrostrain and dislocation density. From the SEM study it was observed that film deposited at 90^0C had well defined crystallites, uniformly distributed over the entire surface of the substrate. The optical study revealed that the optical band gap decreased from 2.26 eV to 1.13 eV as the bath temperature varied from 60^0C to 90^0C

Deposition time also has significant effects on structural, morphological and optical properties of thin films deposited by CBD. Experimental studies also show those effects, Barote Maqbul et al. [18] varied the deposition time between 30 min. to 90 min and show the variation of film thickness with deposition time. Initially, PbSe film thickness was increased linearly up to 70 min. and slightly decreased for further deposition time. The maximum thickness of the PbSe film was found to be 335 nm and further film thickness decreased due to dissolution of film in the solution. The thickness of the film is increased by retreating the samples, each time to fresh quantities of the solutions. as thickness of the sample increases from 335nm to 638nm with deposition time and the grain size also

increases from 10nm to18nm. In addition to that P. Aggrawal et al. [19] study shown that the grain size of the CdSe film has increased from 4.4nm to 5.9nm as the deposition times are increased from 60min to 150 min. Recently in 2021 Effect of Deposition Time on Structural and Optoelectronic Properties of Flower-Like Nanostructured PbS Thin Films studied by N. H. Sheeba et al [20] and their Optical studies indicate a slight decrease in bandgap energy with increase in deposition time which is in the range 1.65 - 1.41 eV. The three PbS samples in this study exhibit similar pattern of variations with different properties discussed which clearly indicate that complete formation of PbS takes place in sample PbS-2 at a growth time of 3 h. On further increasing the dip time to 6 h, very slight improvement in the quality of films is observed. Hence PbS-2 that grown at 3 h dip time is opted as the suitable.

3.1.4. Thin film characterization

Thin films may characterize with different methods respectively to their properties as broad classification some of methods revised as follow. [21]

Film Thickness: optical methods for Film thickness determinations are widely used for a number of reasons. They are applicable to both opaque and transparent films, yielding thickness values of generally high accuracy. In addition, measurements are quickly performed, frequently nondestructive, and utilize relatively inexpensive equipment. The single basic principle which most optical techniques rely on is the interference of two or more beams of light whose optical path difference is related to film thickness. For instances, Interferometry of opaque films (Fringes of equal thickness (FET), Fringes of equal chromatic order (FECO)), Interferometry of transparent films, a perfectly suitable method for measuring the thickness of transparent films is to first generate a step, metalize the film-substrate and then proceed with either the FET or FECO techniques. Some of mechanical techniques are Stylus-method profilometry, weight measurement crystal oscillators

Structural Characterization: Among those methods to characterize physical properties of thin film

Scanning Electron Microscopy (SEM), is a type of electron microscope that produce images of sample by scanning the surface with a focused beam of electrons. The electrons interact with atoms in a sample produce various signals that contains information about the surface topology and composition of sample

Transmission Electron Microscopy (TEM)**:**is used to obtain structural information from specimens that are thin enough to transmit electrons, X-Ray Diffraction (XRD): X-ray diffraction is a very important experimental technique that has long been used to address all issues related to the crystal structure of bulk solids, including lattice constants and geometry, identification of unknown materials, orientation of single crystals, and preferred orientation of polycrystals, defects, stresses, etc.

3.2 Computational

3.2.1 Basics of DFT

A. Born-Oppenheimer Approximation

The electronic structure of a material is in principle obtained by solving the Schrödinger Equation $H\Psi = H\Psi$ of the system described by the wave-function), $\Psi(R\ ;\ r)$ of interacting electrons (with positions r) and nuclei (with positions R). Such a many-body problem can, however, not be solved exactly and one usually assumes that the movement of the electrons can be decoupled from the movement of the nuclei. It is the Born-Oppenheimer approximation, justified by the much greater velocities of the electrons compared to the velocities of the heavier nuclei: electrons respond quasi instantaneously to the movement of the nuclei and one can consider that electrons remain in their ground state during the displacement of the nuclei. As a consequence, the electron wave-function) $\Psi(r)$ is determined for fixed positions R of the nuclei and the dependence in R can be omitted. This approximation can be considered valid in most cases and in particular as long as the electron-phonon coupling is not fundamental in the properties studied. The Hamiltonian H

of the system therefore becomes that of interacting electrons moving in the external field created by the nuclei.

- Mass of nuclei exceeds that of the electrons by a factor of 1000 or more so that
  - we can neglect the kinetic energy of the nuclei
  - treat the ion-ion interaction classically
  - significantly simplifies the Hamiltonian for the electrons

Consider Hamiltonian for *n* electrons in potential of *N* nuclei with atomic numbers *Z*

$$H = -\frac{\hbar^2}{2m}\sum_{i=1}^{n}\nabla_{\mathbf{r}_i}^2 - \sum_{i=1}^{N}\sum_{j=1}^{n}\frac{Z_i e^2}{\left|\mathbf{R}_i - \mathbf{r}_j\right|} + \frac{1}{2}\sum_{i=1}^{n}\sum_{\substack{j=1\\ i\neq j}}^{n}\frac{e^2}{\left|\mathbf{r}_i - \mathbf{r}_j\right|} \quad \text{.........................(3.3)}$$

Where the midterm External potential $V_{ext}(\boldsymbol{r}_j)$

B. The Solution of the Schrödinger Equation

The ground state energy of a collection of atoms. The energy may be computed by solution of the Schrödinger equation – which, in the time independent, nonrelativistic, Born-Oppenheimer approximation is [22]

$$\hat{H}\Psi(r_1, r_2, \dots\dots, r_{n,}) = E\Psi(r_1, r_2, \dots\dots, r_{n,}) \quad \text{...................... (3.4)}$$

The electronic Hamiltonian operator, H, consists of a sum of three terms; the kinetic energy, the interaction with the external potential (V_{ext}) and the electron-electron interaction (V_{ee}). That is;

$$\hat{H}_e = -\sum_i \frac{1}{2}\nabla_i^2 + \frac{1}{2}\sum_{i\neq j}\frac{e^2}{|r_i - r_j|} - \sum_{i,n}\frac{Z_n}{|r_i - R_n|}, \text{ respectively} \quad \text{......... (3.5)}$$

The Hamiltonian operator consists of single electron and bi-electronic interactions – i.e., operators that involve on the coordinates of one or two electrons only. In order to compute the total energy, we do not need to know the 3N dimensional wave function. Knowledge of the two-particle probability density – that is, the probability of finding an electron at r_1 and an electron at r_2 is sufficient.

C. Hohenberg-Kohn theorems

The beauty and power of the so-called Density Functional Theory relies on two very simple theorems, known as Hohenberg-Kohn theorems [23], whose results can be summarized as follow in studying ground-state electronic properties one can replace the ground-state electronic wave function $\Psi\left(x_1, x_2, \dots \dots, x_{n,}\right)$ with the simple electron density n(r). In other words, one can use the electron density as fundamental variable: the ground-state wave function (and therefore any ground state property) is a functional of the electron density, Ψ = Ψ[n].

These properties follow from two very simple theorems

Theorem I: The density 'n' uniquely determines 'V', that is $V = V[n]$ or, in other words, for each electron density; n, there exists one and only one potential V.

$$E = E[n(r)] \quad \dots\dots\dots\dots\dots\dots \quad (3.6)$$

Theorem II For any given external potential V a density variational principle can be formulated, i.e. there exist a functional, called "energy functional" E [n] such that

$$E[n(r)] \geq E_0[E_0(r)] \quad \dots\dots\dots\dots\dots\dots \quad (3.7)$$

Where, E_0 is the ground-state energy. The equality sign holds if and only if n is the ground-state density.

The ground-state wave function, ψ[n], for the potential υ(r) is itself a functional of n, which was exploited by Hohenberg and Kohn to define the universal (i.e., independent from the external potential) density functional, as

$$F[n] = \langle \psi[n] | \hat{T} + \hat{V}_{ee} | \psi[n] \rangle \quad \text{.............................. (3.8)}$$

which can be used to define the total electronic energy functional expressed as

$$E[n] = F[n] + E_{ext}[\mathrm{n}] \quad \text{........................... ....(3.9)}$$

Can be expressed as $E[n] = F[n] + \int v_{ne}(\boldsymbol{r})n(\boldsymbol{r})$............................(3.10)

Where the first term, the universal functional contains the individual contributions of kinetic energy, classical Coulomb interaction, and the non-classical self-interaction correction and the second term external energy, E_{ext}[n], for the specific external potential V_{ne}[r],

So that the energy functional further expressed as

$$E[n] = T[n] + E_{int}[n] + E_{ext}[n] \quad \text{............................. (3.11}$$

D. Kohn–Sham equation

Kohn–Sham equation is the one-electron Schrödinger equation of a fictitious system (the "Kohn–Sham system") of noninteracting particles (typically electrons) that generate the same density as any given system of interacting particles.[24][25]
The Kohn–Sham equation is defined by a local effective (fictitious) external potential in which the non-interacting particles move, typically denoted as v_{eff}, called the Kohn–Sham potential. As the particles in the Kohn–Sham system are non-interacting fermions, the Kohn Sham wavefunction is a single Slater determinant constructed from a set of orbitals that are the lowest-energy solutions to

$$\left(-\frac{\hbar^2}{2m}\nabla^2 + v_{eff}(\mathbf{r})\right)\varphi_i(\mathbf{r}) = \varepsilon_i\varphi_i(\mathbf{r}) \quad \ldots\ldots\ldots\ldots\ldots\ldots\ldots\ldots\ldots (3.12)$$

E. The Energy Functional

KS decomposition the total energy of a many electron system in an external potential is

$$E[n] = T_0[n] + \frac{1}{2}\iint \frac{n(r)n(r')}{|r-r'|}drdr + \int v_{ne}(\boldsymbol{r})n(\boldsymbol{r})d\boldsymbol{r} + \int \varepsilon_{XC}[n(\boldsymbol{r})]n(\boldsymbol{r})d\boldsymbol{r} \ldots\ldots (3.13)$$

or

$$E[n] = T_s[n] + \int d^3r V_{ext}(\vec{\boldsymbol{r}})n(\vec{\boldsymbol{r}}) + E_H[n] + E_{XC}[n] \quad \ldots\ldots\ldots\ldots\ldots\ldots (3.14)$$

Can be also express as;

$$E[n] = T_0[n] + E_H[n] + E_{ext}[n] + E_{XC}[n] \quad \ldots\ldots\ldots\ldots\ldots\ldots\ldots\ldots (3.15)$$

$T_0[n]$, The kinetic energy of the fictitious non-interacting electrons functional

$E_H[n]$ is classical coulomb energy,

$$E_H[n] = \frac{1}{2}\int\int\ dV\ dn' \frac{n(r)n(r^1)}{|r-r^1|} \quad \text{.......................... (3.16)}$$

$E_{ext}[n]$, external energy and $E_{XC}[n]$ exchange and correlation energy

F. The Exchange-Correlation energy functional

The exchange-correlation energy $E_{XC}[n]$ was introduced as a remaining between the unknown exact energy functional $E[n]$ and the sum given by the kinetic energy of the non-interacting electron gas at the same density, plus the Hartree term and the contribution of the external potential (see eq above). $E_{XC}[n]$can be defined as:

$$E_{XC}[n] = E[n] - E_{known}[n] \quad \text{.............................. (3.17)}$$

Therefore, $E_{XC}[n]$ should account for all the purely quantum effects, namely exchange and correlation

$$E_{known}[n] = T_s[n] + \int d^3 r V_{ext}(\vec{\boldsymbol{r}})n(\vec{\boldsymbol{r}}) + E_H[n] \qquad \text{............ (3.18)}$$

correlation, and eliminate the spurious electron self-interaction term that is present in $E_H[n]]$ as well. Note that $E_{XC}[n]$is simply a functional of the electron density and is independent of the external potential, so that it should work for all materials.

G. Approximations

The Local Density Approximation:

For electron densities that are uniform in space

$$E_{XC}^{HEG}(n) = V\frac{N}{V}e_{XC}^{HEG}(n) \quad \text{……………….……….} \quad (3.19)$$

Where, $e_{XC}^{HEG}(n)$ is the exchange-correlation energy per electron in the homogeneous electron gas [26]

For electron densities that are not uniform in space. Let's assume that the functional dependence of E_{XC} on $n(\vec{\boldsymbol{r}})$ is the same as in the HEG, in order to obtain the LDA approximation:

$$E_{XC}^{LDA}[n] = \int d^3r\, n(\vec{\boldsymbol{r}})e_{XC}^{HEG}(n(\vec{\boldsymbol{r}})) \quad \text{…….………………….} \quad (3.20)$$

where we have replaced n with the local density $n(\vec{\boldsymbol{r}})$ at the point $(\vec{\boldsymbol{r}})$ and the volume V with the sum of small cells in which the system is supposed to be homogeneous. As a consequence, the LDA is expected to be a good approximation for systems in which the electron density does very little and not too rapidly.

The Generalized Gradient Approximation:

In the generalized gradient approximation (GGA) a functional form is adopted which ensures the normalization condition and that the exchange hole is negative definite [27,28]. This leads to an energy functional that depends on both the density and its gradient but retains the analytic properties of the exchange correlation hole inherent in the LDA.
The typical form for a GGA functional is;

$$E_{XC}^{GGA}[n] = \int \varepsilon[n(\boldsymbol{r}).|\nabla n(\boldsymbol{r})|]\, d\boldsymbol{r} \quad \text{...……….…………...} \quad (3.21)$$

3.2.2. Practical Implementation

Bloch theorem: By considering all of our DFT calculations to be done in a solid, i.e. a system with discrete translational invariance. This implies that we can use the Bloch theorem. The advantages of using the Bloch theorem are The Hamiltonian is diagonal in $\vec{k}$ and to the calculations can be restricted to a single unit cell

Using Bloch theorem, equation (3.11) is expressed in the Bloch basis, and defines the dispersion relationship $\epsilon_{\vec{k}}$

$$\left(-\frac{\hbar^2}{2m}\left(\frac{1}{i}\Delta+\vec{k}\right)^2+v_{scf}(\vec{\boldsymbol{r}})\right)u_{\vec{k}}(\vec{\boldsymbol{r}})=\epsilon_{\vec{k}}u_{\vec{k}}(\vec{\boldsymbol{r}}) \quad \ldots\ldots\ldots\ldots\ldots (3.22)$$

where $\vec{k}$ is a wave vector belonging to the first Brillouin zone and v_{scf} and $u_{\vec{k}}(\vec{\boldsymbol{r}})$ are lattice-periodic functions [29]. Solving single particle equation also we can evaluate with different value of K as the Hamiltonian is already diagonal in $\vec{k}$. For each given $\vec{k}$ we will get a set of $\epsilon_i(\vec{k})$, which is our dispersion relationship.

Energy Cutoff: Equation (20) is still a second order differential equation, which needs to be solved numerically. The easiest way to do it is instead of directly solving the solution, we can expand the wave function as a sum of basis set functions, weighed with a coefficient Then the correct solution is found if one finds the right coefficients, i.e., if one solves a linear system, which is much easier to do in a machine. In principle one has to consider an infinite sum of basis set functions. In Quantum Espresso the expansion is done in terms of plane waves. So, a cut off energy value, determines the number of plane waves in the expansion

Pseudopotential

The pseudopotential approximation was first introduced by Hans Hellmann in 1934.[30] The pseudopotential is an attempt to replace the complicated effects of the motion of the core (i.e. non-valence) electrons of an atom and its nucleus with an effective potential, or pseudopotential. which allows one to greatly reduce the number of plane waves needed, without changing the chemical properties of the atoms Pseudopotentials with larger cut-off radius are said to be softer, that is more rapidly convergent, but at the same time less transferable, that is less accurate to reproduce realistic features in different environments.

Brillouin zone [Bz] sampling

We need to compute with involvement an integral over the BZ. For computational purpose, sampling is done over the first BZ (which is a 3D solid) with a discrete k-point grid (Monkhorst-Pack grid).

As the size of the system increases, the k points become dense in the BZ and tend to be infinite for a truly unbound crystal. Clearly, there are computational restrictions that prevent the use of a too large set of $\vec{k}$ points. The choice of an optimal infinite set is often referred to as BZ sampling.

In order to reduce the number of k points needed, the code typically introduces a smearing on the occupations, such as the Fermi function at T = 0, $T \neq 0$ or a Gaussian broadening. Imagine that for every sum involving δ functions, we sum over a Gaussian instead. This helps to greatly speed up convergence. Values between 0.01 and 0.08 Ry are reasonable for the self-consistent calculation. The larger the smearing, the less the $\vec{k}$ points needed, and the faster the calculation. Values too large, however, may give wrong results, especially in semiconductors where the conduction band may become occupied. As a first guess, try with0.05 Ry. [31]

3.2.3. Quantum Espresso

Quantum opEn-Source Package for Research in Electronic Structure, Simulation, and Optimization,[31]

The main goals of Quantum ESPRESSO (QE) are

- innovation in theoretical methods and numerical algorithms
- efficiency on modern computer architectures

Advantages:

- Everybody – including commercial entities – can contribute.
- Nobody can "steal" the code and give nothing back to the community

Software Packages

QE is not a monolithic code, it is composed of several packages

PWscf: self-consistent electronic structure, (variable-cell) structural optimization, molecular dynamics, **CP**: Car-Parrinello molecular dynamics, also with variable cell They share a common installation method, input format, pseudopotential format, data output format, large parts of the basic code. **Dos**: A small script which sums over the eigenvalues obtained by pw to get the density of states, **bands**: Another small script which collects the output of a special pw calculation, and produces a data file to plot the bands More packages:

PHonon: linear-response calculations (phonons, dielectric properties). **PostProc**: graphical and post processing utilities (density of states, STM, etc.), **PWneb**: Nudged Elastic Band (NEB) for reaction pathways and barriers, **atomic**: pseudopotential generation code and **PWGui**: a Graphical User Interface for production of input files

Structure of Input Files: Quantum Espresso's input file consists of 3 major sections (&control, &system, &electrons) and 2 optional sections (&ions, &cell) depending on the type of calculation to be performed additional information about your molecule or the

crystal system has to be specified such as atomic species, atomic positions, k-points and cell parameters.

3.3. Experimental Procedures and Computational Details

3.3.1 Experimental procedures

Lead sulfide thin films were synthesized by chemical bath deposition method on glass substrate at a bath temperature of 80 ^{0}C. The precursors lead acetate trihydrate ($PbC_4H_6O_4$.$3H_2O$), gallium nitrate hydrate ($Ga(NO_3)$) and thiourea ($CS(NH_2)_2$ were used as lead, gallium and sulfur ions source respectively. Hexamethylenediamine ($NH_2(CH_2)_6NH_2$) was used as complexing agent. Before the deposition process 0.25 M of each precursors were dissolved by distilled water individually in 100 mL volume flask. Pure PbS thin film was prepared following the following procedure: 7 ml lead acetate trihydrate solution was added in to 100 ml beaker under continuous string. Then 10 ml of $NH_2(CH_2)_6NH_2$ added slowly in to the above solution. The pH of the chemical bath was adjusted around 11 by adding 10 ml aqueous ammonium hydroxide (NH_3 aq.). It was noticed that adding NH_3 is necessary to dissolve excess $Pb(OH)_2$ formed upon mixing the lead acetate with sodium hydroxide. Finally, 7 ml of ($CS(NH_2)_2$) added and maintained the total chemical bath about 65 ml by adding appropriate amount of distilled water. Ga doped PbS thin films prepared by the same procedure adjusting volumetric percentage concentration of gallium nitrate solution (2, 4, 6, 8, 10 and 15 %) relative to $PbC_4H_6O_4$.$3H_2O$. In all cases the solution color changed to dark brown after 4 min. After 25 min deposition time the substrate was taken out of the bath and rinsed several times with distil water and then kept and dried for further characterizations. The prepared thin films were characterized by varieties of techniques. The structural study carried out by XRD of Bruker D8 advance diffractometer with Cu-K_α (1.5406 Å). The machine was operated at 40 mA and 40 kV. The optical absorption spectra were measured using a Perkin Elmer Lambda 950 UV–Vis–NIR Spectrophotometer within the wavelength range of 250–2000 nm. The room temperature photoluminescence (PL) measurements were carried out by Horiba Fluoroma-4 Spectrofluorometer.

3.3.2 Computational Details

Structural and electronic properties of pure and Ga doped PbS were computed using DFT via Quantum-ESPRESSO (QE) software package. Two pseudopotentials (PP) with in different XC-functional groups Perdew-Burke-Ernzerhof (PBE) and Perdew-Burke-Ernzerhof for solid (PBEsol) were applied in the QE input file to optimize their performance Total energy convergence test with k-point was made and optimized value of k-point grid 4x4x4 was chosen, moreover, from the suggested PP, 413.717 Ry cutoff charge and 45.9686 Ry cutoff energy values were sets and employed in all the subsequent calculations. Doping of Ga in PbS molecule needs some arrangement in geometrical cluster by creating supercell. This helps us to manage the Ga percentage composition for doping purpose. A 2 x 2x 2 transformation face centered cubic (FCC) (2 number of atoms per cell) to FCC which has 16 number of atoms was made to dope 12.5%, 25%, 37.5%, and 50% Ga on PbS. ($Pb_X Ga_Y S_8$) where, x = 7,6,5,4; y = 1,2,3,4 represents number of atoms of Ga and Pb participation in the unit cell. We have set Monkhorst and Pack (MP) mesh k-point to 4 x 4x 4 for all self-consistent calculations and 12 special k-points (Γ – X – W – K – Γ – G – L – U - W- L - K|U - X) for band structure calculations as those are suggested k-path for FCC lattice. Due to the super cell created, the lattice parameter is doubled (12 Å) while the MP k-point is reduced by half (2 x 2x 2). The effects of doping of Ga on the properties of PbS in each concentration are then studied.

CHAPTER 4

Result and Discussion

4.1 Experimental Results

4.1.1. Structural analysis

The structural properties of Ga doped and undoped PbS thin films were studied by using XRD. The study reveals the polycrystalline nature of PbS and Ga- doped PbS. The well-defined peaks orientation was observed along the (111), (200), (220), (311), (222), (400), (331), (420) and (422) planes (See Figure 4.1). As a consequence of Ga impurity, non-uniform Bragg's angle θ shift was observed. It's preferable to group significant peaks in to two, depending on their shift direction on θ. The right major peak and left side major peak Ga (2 and 6 %) are right side major peaks and Ga (8 and 10%) are left side major peaks along both the (111) and (200) planes. Separately here the peak shift to the right (higher) angle θ for Ga (2 and 6%) concentration but for Ga (4 and 8%) the peak shifted to the left (smaller) angle θ from their previous states. For Ga (8, 10 and 15%) concentration, the peaks shift to relatively larger angle θ sequentially even though all three peaks lie to the left side of the undoped PbS peak. As the relations between lattice parameter and Brag's angle θ shown in Eqn. 4.1 and Eqn. 4.2 small angle θ means large d, which also increase a_{hkl} this means all the left shift indicates increment of lattice constant and vice versa. The peak shift towards the left side may due to the diffusion of additional Ga atom with in PbS unit cell results the expanding of the cell volume. The other observation was that the peak shift to the larger angle θ this shows the lattice parameter of host atom reduced this due to the Substitution of Ga atom which has small atomic radius than Pb results the unit cell volume to be shrink. More over the effect of Ga impurity on the intensity of diffraction peaks was observed clearly as shown in Figure (4.2b and 4.2c) for more detail view of plane (111) and (200), which are the most two preferable planes that high peaks were observed. from 2% - 8% Ga concentration, the highest peak was visible along (111) plane whereas for Ga 10% both peaks were high at (111) and (200) planes. finally, at Ga 15% the high peak completely aligns with to (200) plane. The observation of such peak intensity

variation was due to the change in crystallite behavior of host atom as the consequence of Ga impurity. This phenomenon indicates Ga impurity cause change in grain growth direction.

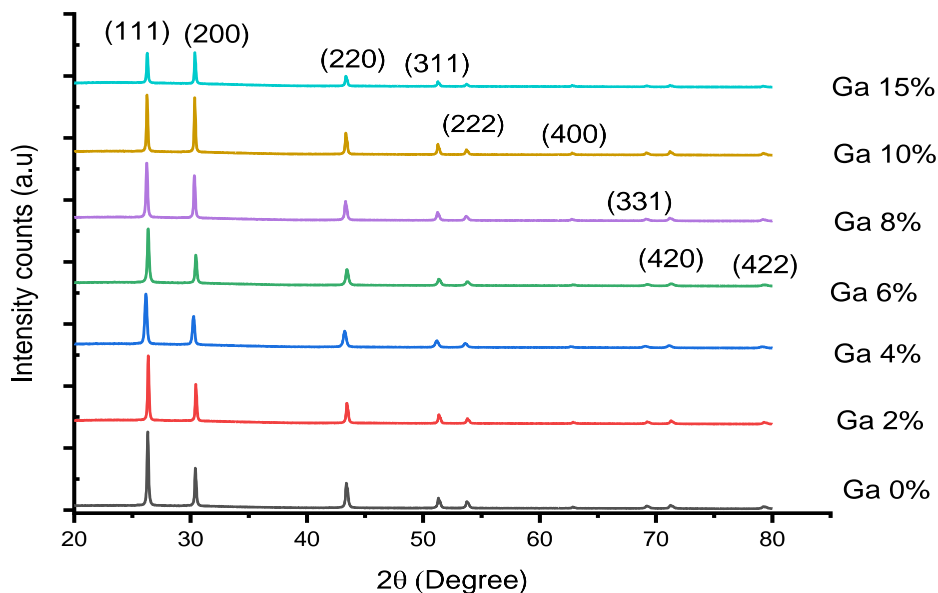

Figure 4.1. The XRD pattern of PbS and Ga doped PbS thin films for different Ga concentration.

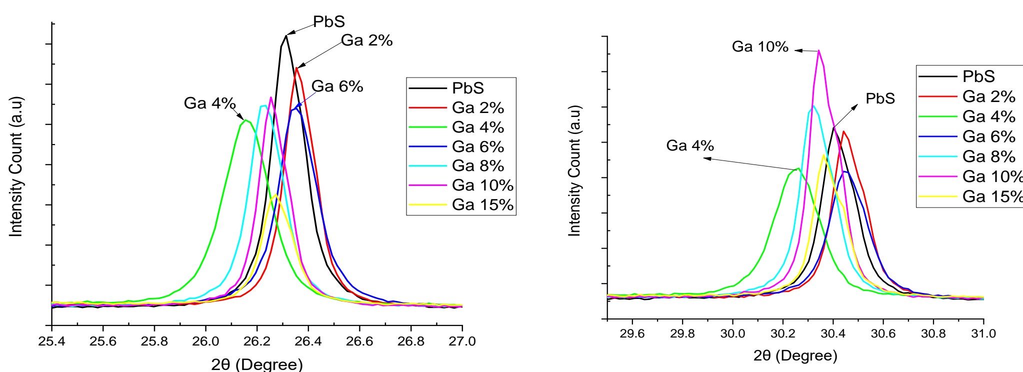

(a). (b).

Figure 4.2. Extended X-ray diffraction patterns of the A. (111) and B. the (200) plane peaks for pure and Ga doped PbS thin films.

To determine the lattice constant the relation in equation. (4.1) was used.

$$a_{hkl} = d_{hkl}\sqrt{h^2 + k^2 + l^2} \quad \text{......................................} \ 4.1$$

Where, a is lattice parameter, d is interplanar spacing or d-spacing and (h, k, l) are miller indices. we use standard card number (PbS JCPDS 05-0592) to indices the XRD major peaks.

d also obtained by using Bragg's equation (4.2)

$$n\lambda = 2d\sin\theta \qquad \text{......................................} 4.2$$

Where, n is order of diffraction (1), λ is wavelength of incident X-ray (1.5406 Å) and θ is peak position in Radian. Bragg's angle θ found from the analyzed peak positions of intensity versus 2θ graph (Figure 4.1).

Crystalline size D calculated by using Scherrer equation (eqn.4.3)

$$D = \frac{k\lambda}{\beta\cos\theta}\ , \text{D} \ll 200\text{nm} \qquad \text{.................................} \ (4.3)$$

Where, D is the crystallite size, K is Scherrer constant its value is 0.94 for spherical crystallites with cubic symmetry, β is line broadening at FWHM in radians and θ is the Bragg's angle in degree

Dislocation density, (δ) and Micro strain (ε) calculated by (eqn.4.4 and 4.5) respectively

$$\delta = \frac{1}{D^2} \quad \text{...} (4.4)$$

$$\varepsilon = \frac{\beta}{4 \tan \theta} \quad \ldots\ldots\ldots\ldots\ldots\ldots\ldots\ldots (4.5)$$

The calculated values of d-space and lattice constant for undoped PbS and Ga doped PbS for both (111) and (200) orientation with the standard value is in the Tables 4.1 and 4.2. The results calculated for each of nine plane of available X-ray diffraction peaks.

Table 4.1. X-ray diffraction parameters of the undoped and Ga- doped Pbs films from the (111) orientation.

Ga- doping concentration (at.%)	**d-spacing (Å)**		**Lattice constant (Å)**		**N**	**D (nm)**	**Strain (ε) lines^{-2}m^{-4}**	**Dislocation density (δ) lines/ m^2**
	standard	**calculated**	**standard**	**calculated**				
0	3.429	3.384	5.936	5.862	3.85	47.81	0.333 x10^{-3}	4.375 x10^{14}
2	3.429	3.379	5.936	5.853	3.84	50.57	0.314 x10^{-3}	3.910 x10^{14}
4	3.429	3.404	5.936	5.897	3.92	33.57	0.477 x10^{-3}	8.874 x10^{14}
6	3.429	3.379	5.936	5.853	3.84	40.09	0.396 x10^{-3}	6.221 x10^{14}
8	3.429	3.394	5.936	5.879	3.89	44.81	0.356 x10^{-3}	4.980 x10^{14}
10	3.429	3.392	5.936	5.875	3.88	52.89	0.301 x10^{-3}	3.574 x10^{14}
15	3.429	3.389	5.936	5.870	3.87	60.96	0.261 x10^{-3}	2.691 x10^{14}

Table 4.2. X-ray diffraction parameters of the undoped and Ga- doped Pbs films from the (200) orientation.

Ga- doping concentration (at.%)	d-spacing (Å)		Lattice constant (Å)		N	D (nm)	Strain (ε) lines^{-2}m^{-4}	Dislocation density (δ) lines/ m^2
	standard	calculated	standard	calculated				
0	3.429	2.938	5.936	5.876	3.88	46.19	0.299 x10^{-3}	4.688 x10^{14}
2	3.429	2.934	5.936	5.868	3.86	47.65	0.289 x10^{-3}	4.405 x10^{14}
4	3.429	2.951	5.936	5.913	3.95	34.30	0.404 x10^{-3}	8.502 x10^{14}
6	3.429	2.934	5.936	5.868	3.86	40.19	0.343 x10^{-3}	6.191 x10^{14}
8	3.429	2.945	5.936	5.891	3.91	47.46	0.292 x10^{-3}	4.439 x10^{14}
10	3.429	2.943	5.936	5.887	3.90	53.29	0.260 x10^{-3}	3.522 x10^{14}
15	3.429	2.941	5.936	5.883	3.89	54.01	0.256 x10^{-3}	3.428 x10^{14}

The calculated lattice parameter of undoped PbS corresponding to (100) and (200) orientation described in tables 4.1 and 4.2 was found 5.862 eV and 5.876 respectively, those results may relatively comply with the theoretical value of bulk PbS lattice parameter 5.936 eV. The additive of Ga impurity has a significant effect on the structural parameter of PbS this fact clearly visible in those results, The Ga (2 and 6 %) impurity leads the lattice parameter to decrease but all Ga (4,8,10,15 %) impurities the resulted lattice parameter was larger than the undoped one. From our theoretical knowledge the dopant atom Ga has small atomic radius than Pb atom, due to this fact we would expect decrease in lattice parameter of our material, but except for Ga (2 and 6%) all the other results don't agree with our expectation but also to the fact. This phenomenon may occur due to the diffusion of more Ga^{+3} ion in to PbS unit cell results increasing unit cell volume during the growth process. This argument may support with additional calculation, the number of atoms per unit cell (N)[43]. The number of atoms non uniformly increased from 3.84 to 3.92 and 3.86 to 3.95 for (111) plane and (200) as shown in Table 4.1, and Table 4.2 respectively, increment of lattice parameter observed except for Ga 2% and Ga 6% concentration as the results verified all those increments was due to incorporation of additional number of atom to the pure PbS possibly consists of which is 3.85 or 3.88. at relatively low Ga concentrations Ga

2% up to Ga 8% average crystalline size (D) decreases non linearly from 50.57 to 33.57 nm with increasing Ga concentration. also, we can observe at high Ga concentration (10% and 15%) the film has high crystalline size and is at its respective minimum micro strain and dislocation density. This phenomenon indicated the film becomes more stable. Reports also discussed that increasing internal strain leads increasing crystalline.

4.1.2. Optical analysis

UV data analyzed by Stern relation equation (4.6) to estimate the optical band gap.

$$(Ahv) = [K(hv - E_g)]^{n/2} \qquad \text{.............................(4.6)}$$

Or

$$(Ahv)^2 = K(hv - E_g) \qquad \text{...................................(4.7)}$$

where A is absorption coefficient. K is a constant, n is a constant can be 4 for direct and 1 for Indirect band gap, so n was considered as 1 because is direct band gap. As show Stern plot, Figure 4.3(a, b, c, d. e, f and g) the x intercept of tangent line from $(Ahv)^2$ versus (hv) graph was the estimated optical band gap of undoped PbS and doped with Ga 2%, Ga 4%, Ga6%, Ga 8%, Ga 10% and Ga 15% concentration respectively.

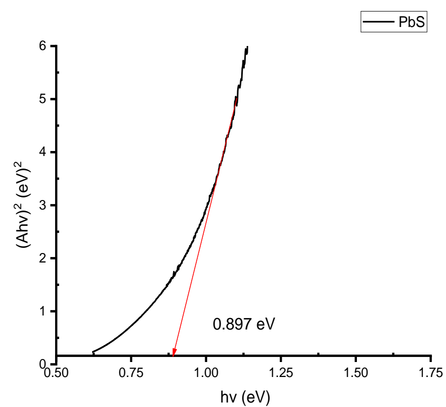

(a)

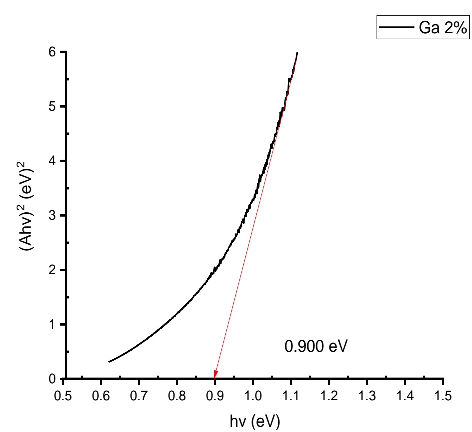

(b)

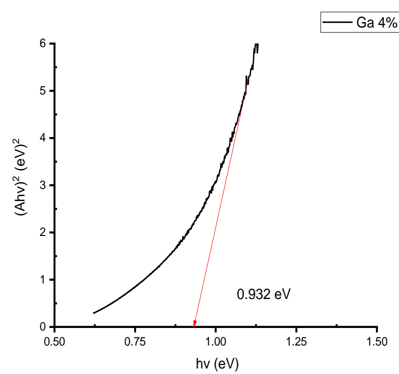

(c)

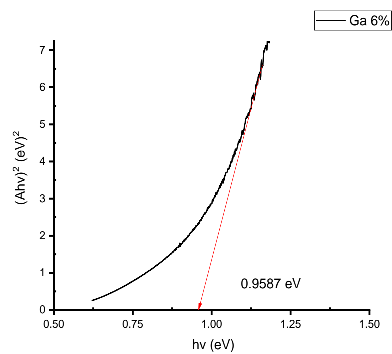

(d)

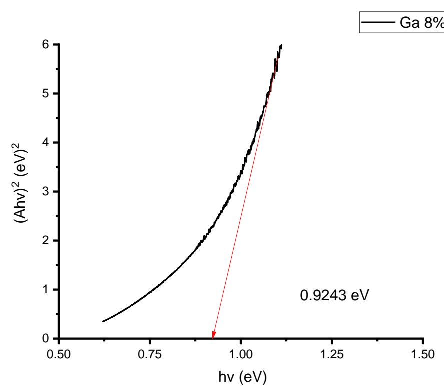

(e)

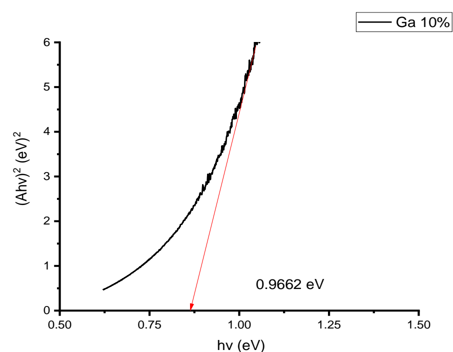

(f)

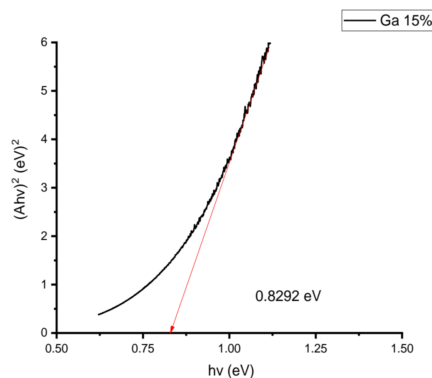

(g)

Figure 4.3. $(Ahv)^2$ vs photoenergy (hv) of undoped and Ga-doped PbS

Table 4.3 Calculated optical band gap of undoped PbS and Ga doped PbS

Ga (%)	Optical band gap (eV)		
	This work (ev)	Other works (eV)	Theoretical (eV)
0	0.897	0.667 [44] 0.900 [49]	0.41
2	0.900	-	-
4	0.932	-	-
6	0.959	-	-
8	0.924	-	-
10	0.966	-	-
15	0.829	-	-

All the result described in (Table 4.3) clearly show the impact of Ga impurity concentration on the optical band gap of Lead Sulfide, the estimated optical band gap of undoped PbS found be around 0.897 eV which is comparable with the result reported by [49], the optical band gap non linearly increased from 0.90 eV up to 0.9662 eV as Ga concentration increase from 2% to 10% The first result (at Ga 2%) shows increase in band gap in fact this was due to decrease in lattice parameter, this result was complied with the theory. Broadening of band gap of PbS by doping appropriate metal also reported in Hone et al [44], Kumar et al. [45] and Portillo Moreno et al1[46]. Justification by Portillo Moreno to such band gap

increment was induced band tailing defect may be the cause for band gap increment due to the formation of localized energy states near the band gap. Additional justification in Rajashree C. [47] Moss-Burstein effect, According to Moss-Burstein effect, this increase in optical band gap may be attributed to an increment of electron in the conduction band by elevating the Fermi level due to dopant elements. Another observation from table 4.3. the lattice constant was increasing due to Ga 4,8,10 % of concentration so those results were not comply with the relation in between lattice constant and band gap. Previously, we have discussed reasons behind this increment of lattice parameter. last one (at Ga 15%) band gap drops down to 0.8292 eV this doesn't expected result but also which is not truly express the of impurity effect.

4.1.3. PL Study

The Photoluminescence study of pure PbS and Ga- doped PbS was caried out at a preferable excitation wave length of 475nm, the emission spectra shown in Figure 4.4 and detail view in Figure 4.5 the peaks observed are at 638.13 nm, 700.93 nm,765.4 nm, 813.51 nm and 830.97 nm. The first emission peak at 638.13 nm may describe the direct transmission from valence to conduction band. The rest of peaks are related to the transition of electrons from the conduction band edge to holes then to valence band. The Ga impurity effect was clearly observed as the intensity peak varies with respective Ga concentration. Low peaks were observed at Ga 2%, 10, and 15% doping concentration which have larger crystallites size (D) this verifies the fact the materials with smaller crystallites size showed higher luminescence intensity compared with the larger crystallites [48], this means the dependency of emission spectra peak to the crystal size was also verified.

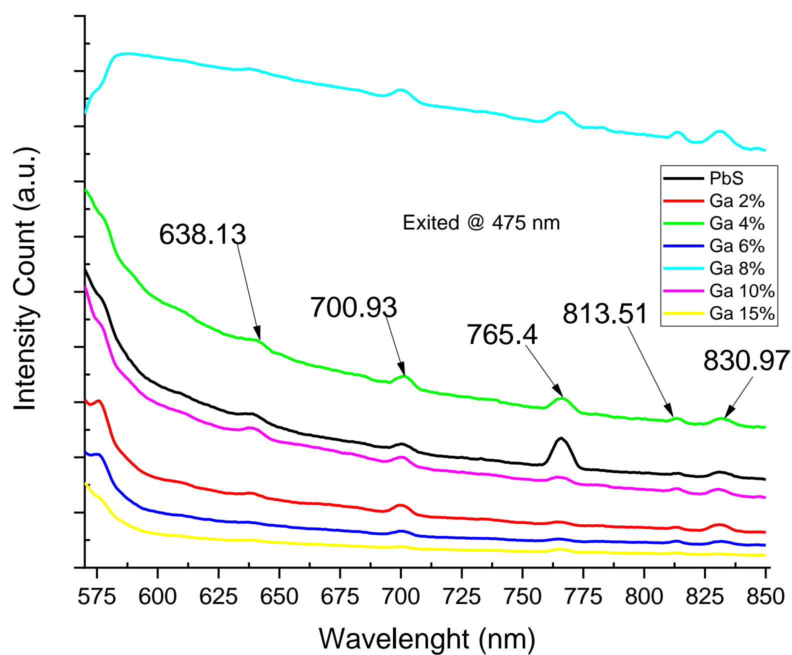

Figure 4.4: Photoluminescence emission spectrum of pure and Ga doped PbS thin films

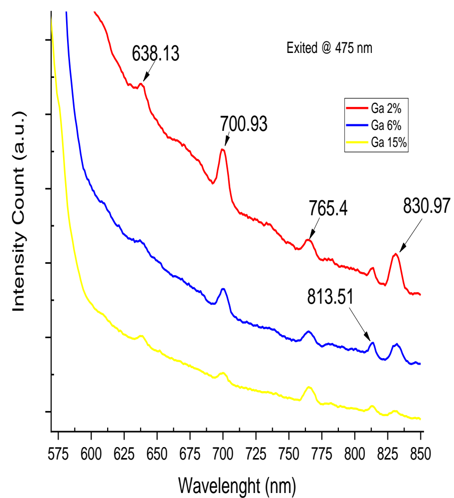

(a)

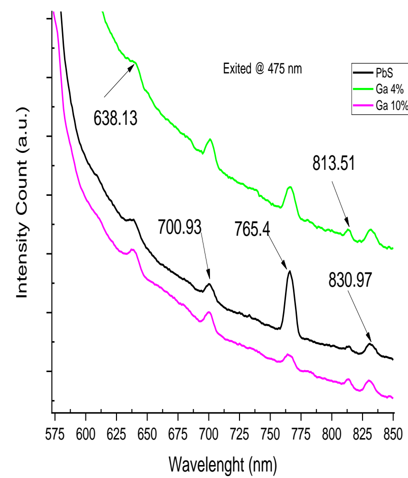

(b)

(c)

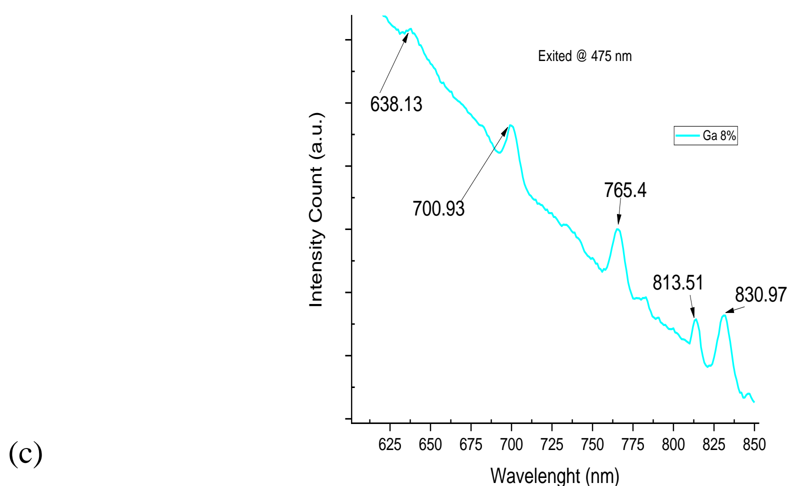

Figure 4.5: Detail view for Photoluminescence emission spectrum of: (a) Ga % of (2,6 and 15), (b) Ga % of (0, 4 and10) and (c) Ga 8% thin film

4.2. Computational Results

Basic information like Bravais lattice type, space group and atomic position of our material are taken from the crystallographic information file (.cif) generated and visualized by visualization for electronic and structural analysis (**VESTA).** Bulk PbS has sodium chloride atom like crystal structure which is FCC crystal structure. A simple cubic model has Bravais lattice of 1 with 8 atoms per unit cell, but for a purpose of simplification Bravais lattice of 2 with two atoms per unit cell Fig. 4.5(a) is used for Bulk PbS calculations. Fig. 1(b), 1(c), 1(d), 1(e), 1(f) shows Supercells of Bulk Lead Sulfide (Pb_8S_8), Ga doped PbS with a concentration of 12.5%, 25%, 37.5 and 50% which means $Ga_1Pb_7S_8$, $Ga_2Pb_6S_8$, $Ga_3Pb_5S_8$,and $Ga_4Pb_4S_8$ respectively.

4.2.1 Structural Properties

Lattice parameter of bulk and Ga-doped PbS ($Ga_xPb_{8-x}S_8$) are calculated as total energy converges with respect to their lattice parameters. The calculated lattice parameters of bulk PbS are 5.913 Å and 6.0 Å for PBEsol and for PBE functional ultrasoft PPs, respectively (See Figs 4.7 (a) and (b)). The lattice parameter of Ga doped PbS is found to decreased with increasing Ga doping as clearly shown in Fig. 4.7. This is due to the fact that the atomic radius of the dopant that substitutes Pb atom is smaller. As the obtained results depicted in Figs. 4.7(c), 4.6(d), 4.6(e), and 4.6(f) shows that the calculated lattice parameter of PbS reduced from 5.9115 Å to 5.7945 Å as the concentration of Ga changes from $Ga_1Pb_7S_8$ to $Ga_4Pb_4S_8$ and the corresponding energy were calculated to each lattice parameter. The lattice parameter together with the corresponding energies obtained computationally, experimentally and theoretically are summarized in Table 4.4.

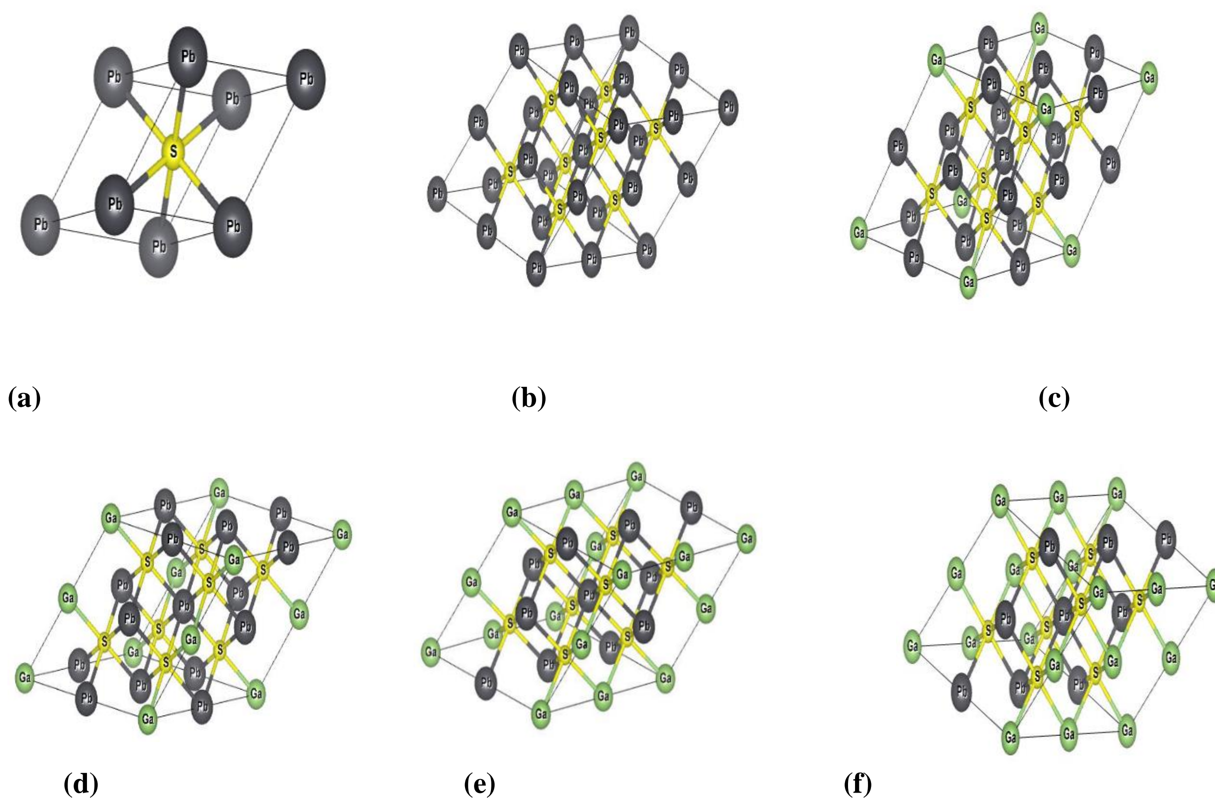

Figure 4.6: Optimized lattice strutueres of (a) pure PbS (b) Pb_8S_8 (c) $Ga_1Pb_7S_8$ (d), $Ga_2Pb_6S_8$, (e) $Ga_3Pb_5S_8$,and (f) $Ga_4Pb_4S_8$

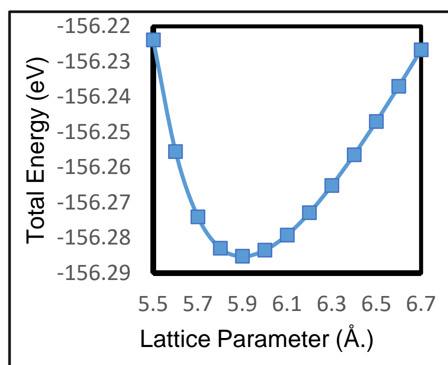

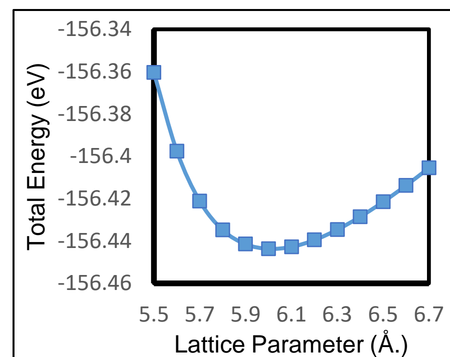

(a) **(b)**

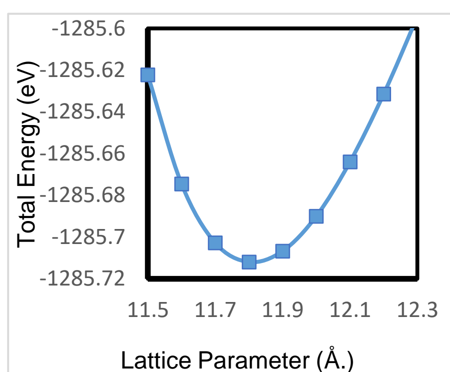

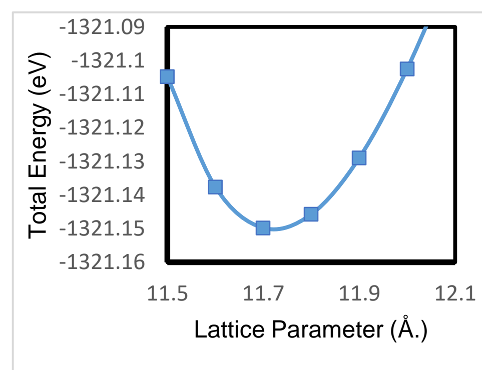

(c) **(d)**

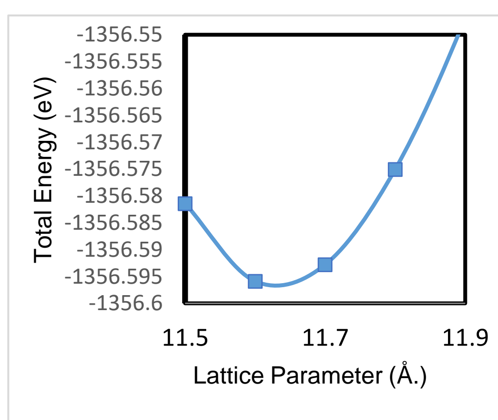

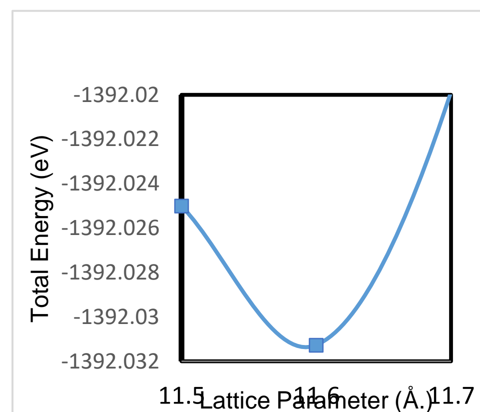

(e) **(f)**

Figure 4.7: Total energy as a function of lattice constant pure PbS with (a) PBEsol (b) PBE functional (c) $Ga_1Pb_7S_8$ (d), $Ga_2Pb_6S_8$, (e) $Ga_3Pb_5S_8$,and (f) $Ga_4Pb_4S_8$

Table 4.4: Results of lattice parameters of PbS, $Ga_1Pb_7S_8$, $Ga_1Pb_7S_8$ $Ga_1Pb_7S_8$ with theoretical experimental, and other DFT calculations

		PbS	$Ga_1Pb_7S_8$	$Ga_2Pb_6S_8$	$Ga_3Pb_5S_8$	$Ga_4Pb_4S_8$
This work	a (Å)	5.913	5.912	5.861	5.815	5.795
	Energy (Ry)	-1250.27	-1285.72	-1321.15	-1356.60	-1392.03
Other work	a (Å)	5.889[50], 6.012[50]	-	-	-	-
	Energy (Ry)	-	-	-	-	-
Experimental	a (Å)	5.950[50]	-	-	-	-
	Energy (Ry)	-	-	-	-	-
Theoretical	a (Å)	5.936[52]	-	-	-	-
	Energy (Ry)	-	-	-	-	

4.2.2 Electronic Property

A. Band structure

Electronic band structure of bulk PbS was simulated using PP with different XC-functional groups. Both PBE and PBEsol studies revealed the direct band gap property of PbS. As shown in Table (4.5), the band gap of PbS calculated using PBEsol XC-functional was 0.3919 eV with 4.414 % error from the theoretical value i.e., 0.41 eV. However, the band gap calculated with PBEsol XC-functional 0.4999 eV with 21.92683 % error than the theoretical value confirming the better performance of PBEsol XC-functional for this particular compound. In regard to the Fermi level, close values around 8.010 eV was found with both XC-functionals. Band structure calculations provide important information about our material. As shown in Fig. 4.7 (a) the minimum gap is created at high symmetry point

lima (L) and; the fermi level is exactly in between the lowest unoccupied (8.4609 eV) and the highest occupied (7.961 eV) energy levels indicating the intrinsic property of PbS. Normalized band structure of PbS and super cell are shown in Fig. 4.7(b) and 4.7 (c). As depicted in Fig. 4.7(c), a minimum gap occurs around special high symmetry point (Γ) as the cell was enlarged to a super cell. The electronic band structure still indicates direct band gap property of Pb_8S_8. The performance of PBE and PBEsol XC-functional on the structure were also tested and a better performance with PBEsol as depicted in Table 4.6. Effects of Ga impurity on PbS compound was systematically studied in concentration percentages of 12.5 %, 25 %, 37.5 % and 50 % with super cell structures having 16 atoms per cell. Ga impurities had significant effect on energy band gap and the Fermi level as shown in Figs. 4.8 and 4.9. The calculation done using PBEsol XC- functional revealed that, the Fermi level goes down below valence band from 7.8038 eV to 7.0996 eV and the concomitant increase of the energy band gap from 0.03543 eV to 0.25789 eV as the concentration of Ga increased from 12.5% to 50%. On the other hand, the calculation done using PBE XC-functional shown in Fig. 4.9, verified that Fermi level goes down below valence band from 8.2002 eV to 7.2404 eV while, the energy band gap increased from 0.04114 eV to 0.26026 eV as the concentration of Ga increased from 12.5 % to 50 %. Effect of Ga-doping on lattice parameter and electronic band gap of PbS are revised in Table 4.7. Similarly, Table 4.8 compared the electronic band gaps of PbS, $Ga_1Pb_7S_8$, $Ga_1Pb_7S_8$, $Ga_1Pb_7S_8$ with theoretical, experimental, and other DFT calculations.

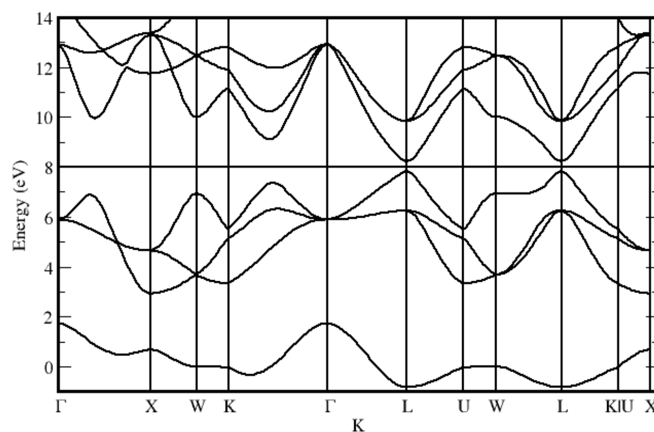

(a

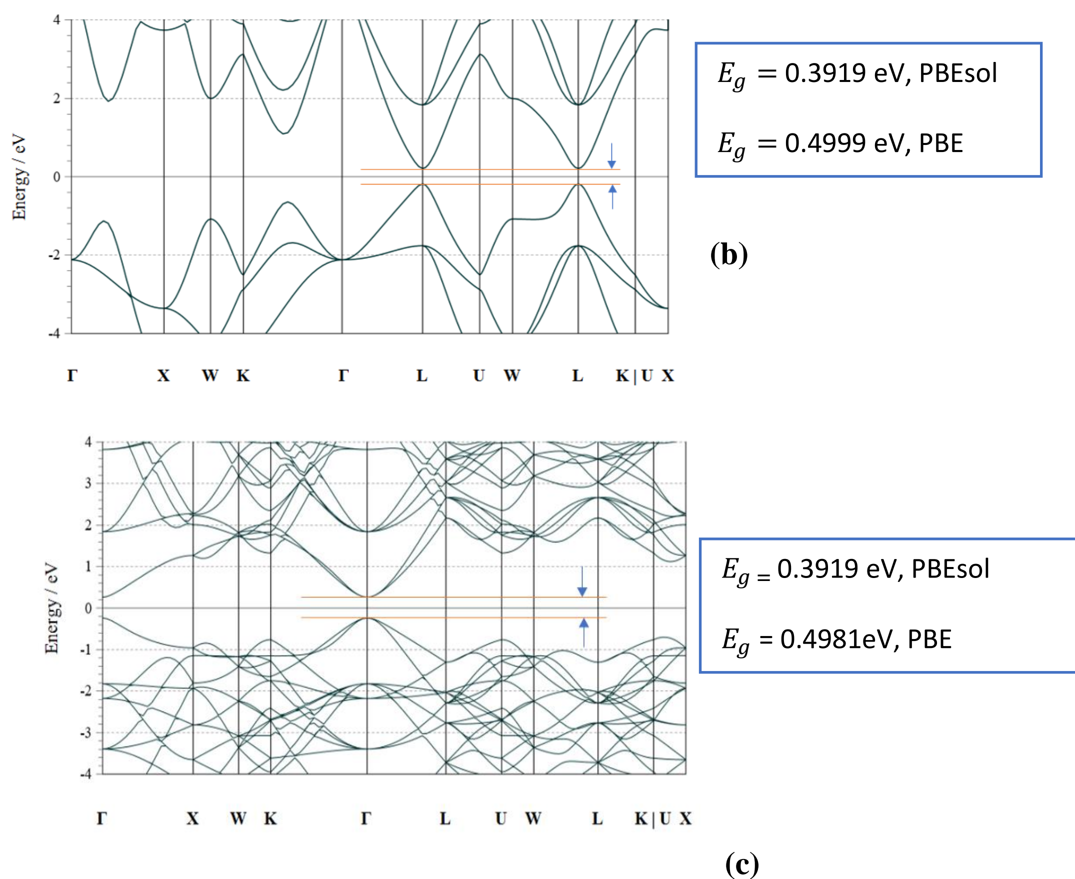

Figure. 4.8: Electronic band structures of PbS (a) with Fermi level (b) Normalized (Fermi level set to 0) (c) Pb_8S_8.

Table 4.5: Performance of PBE and PBEsol functionals on band gap calculation

		Energy Levels		Band Gap	
PP Type	XC-Functional Type	lowest unoccupied	highest occupied	Result	Error (%)
PP	PBE	8.4609	7.9610	0.4999	21.9268
	PBEsol	8.2145	7.8226	0.3919	4.4146

Table 4.6: Effects of Super cell on the band gap

	Fermi level (eV)		Band Gap (eV)	
XC-Functional Type	Normal cell	Supper cell	Normal Cell	Supper cell
PBE	8.2104	8.2110	0.4999	0.4981
PBEsol	8.0178	8.0191	0.3919	0.3919

Table 4.7: Effects of Ga-doping on lattice parameter and energy band gap of PbS

		Lattice	Fermi level		Energy Band Gap	
	PP type	Parameter	PBEsol	PBE	PBEsol	PBE
Pb_8S_8	USPP	5.9130	8.0191	8.2110	0.3919	0.4981
$Ga_1Pb_7S_8$	USPP	5.9115	8.0435	8.2002	0.0354	0.0411
$Ga_2Pb_6S_8$	USPP	5.8610	7.8486	8.0003	0.0458	0.0708
$Ga_3Pb_5S_8$	USPP	5.8145	7.6224	7.7703	0.1972	0.2055
$Ga_4Pb_4S_8$	USPP	5.7945	7.0996	7.2404	0.2579	0.2603

Table 4.8: Results of electronic band gap of PbS, $Ga_1Pb_7S_8$, $Ga_2Pb_6S_8$, $Ga_3Pb_5S_8$ and $Ga_4Pb_4S_8$ with theoretical, experimental, and other DFT calculations.

		This work		Other Works	Experimental	Theoretical
PbS	a (Å)	5.9130		5.8893[50], 6.012[50]	5.950[50]	5.936[51]
	E_g(eV)	PBEsol	0.3919	0.32[52]	0.30[11]	0.41[44]
		PBE	0.4981			
$Ga_1Pb_7S_8$	a (Å)	5.9115		-	-	-
	E_g(eV)	PBEsol	0.0354	-	-	-
		PBE	0.0411			
$Ga_2Pb_6S_8$	a (Å)	5.861		-	-	-
	E_g(eV)	PBEsol	0.0458	-	-	-
		PBE	0.0708			
$Ga_3Pb_5S_8$	a (Å)	5.8145		-	-	-
	E_g(eV)	PBEsol	0.1973	-	-	-
		PBE	0.2055			
$Ga_4Pb_4S_8$	a (Å)	5.7945		-	-	-
	E_g(eV)	PBEsol	0.2579	-	-	-
		PBE	0.2603			

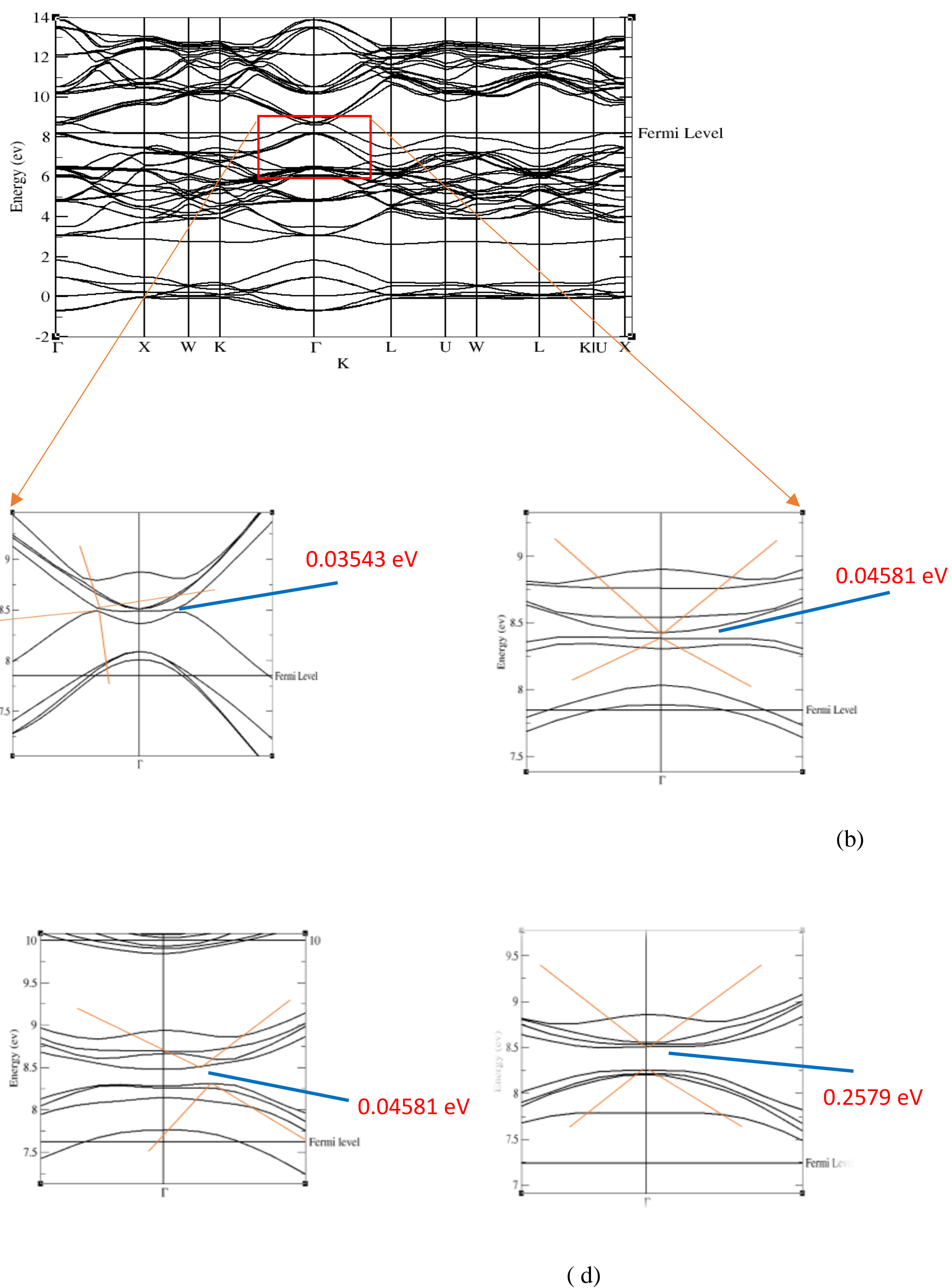

Figure 4.9: Electronic band structure of (a) $Ga_1Pb_7S_8$ (b)$Ga_2Pb_6S_8$, (c) $Ga_3Pb_5S_8$,and (d) $Ga_4Pb_4S_8$ calculated by PBEsol XC functional

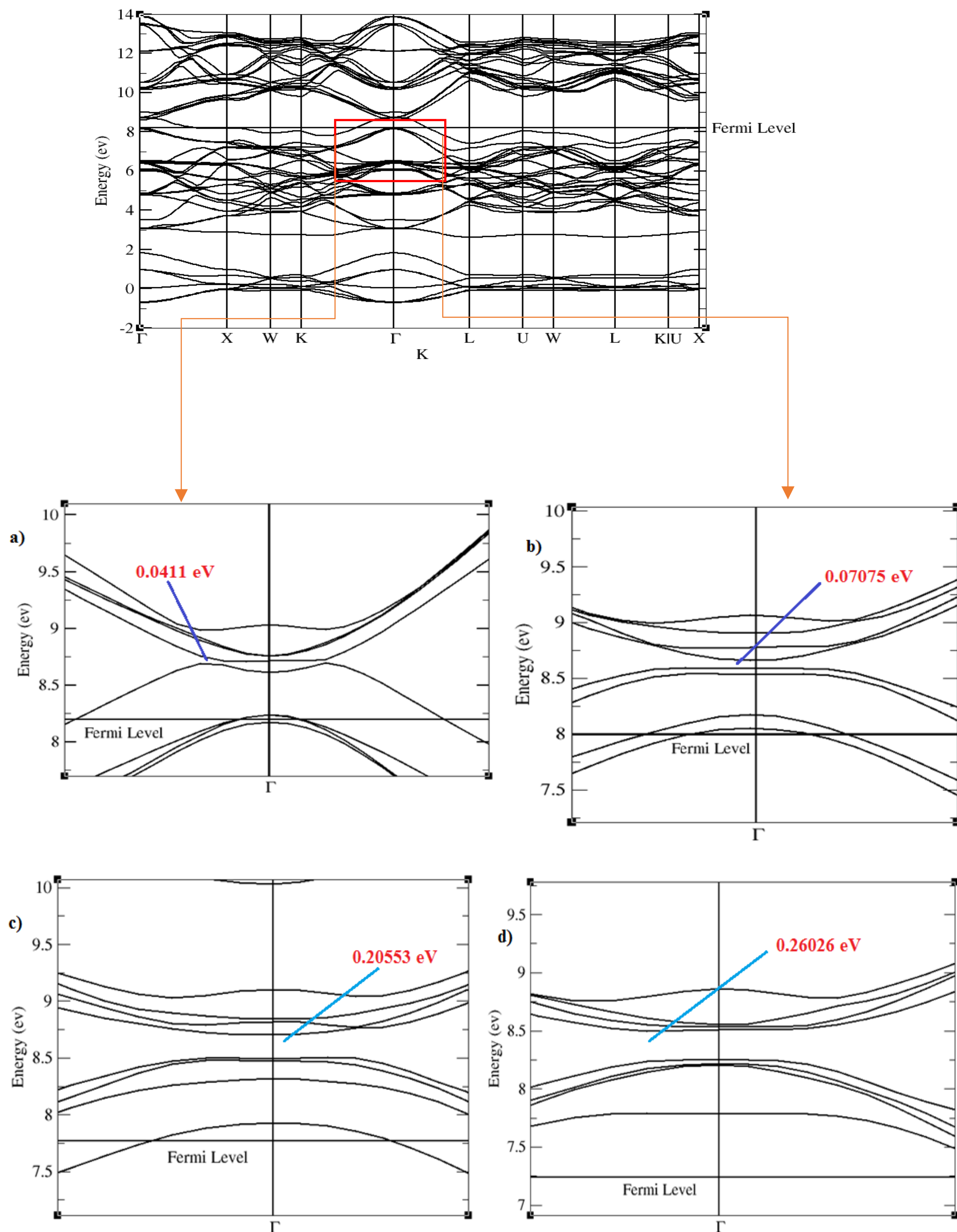

Figure 4.10: Electronic band structure of (a) $Ga_1Pb_7S_8$ (b)$Ga_2Pb_6S_8$, (c) $Ga_3Pb_5S_8$,and (d) $Ga_4Pb_4S_8$ calculated by PBE functional.

B. Density of State (DOS)

Density of states (DOS) describes the number of states of a system per unit interval of energy which are occupied by the electrons. DOS is very important to study band structure property of the system. **DOS of PbS,** Pb_8S_8 , $Ga_1Pb_7S_8$, $Ga_1Pb_7S_8$ $Ga_1Pb_7S_8$ $Ga_1Pb_7S_8$ were studied using PBEsol-functional PP as shown in Fig. 4.10 (a, b), Fig. 4.11, Fig. 4.12, Fig. 4.13 and Fig. 4.14 respectively. There are four regions in the fundamental density of states. The lower region of the valence band (VB), the upper region of VB, the lower region of the conduction band (CB), and the upper region of CB. In our work we were unable to see the upper region of the CB with the reason that the PP we used may consider only the two outer most shall of S (S-p and S-s states). DOS of bulk PbS is shown in Fig. 4.10 (a). The lower part of VB is started around -9 eV and the major contribution at this part is Pb-s state, also a little contribution by the states of S-s S-p and Pb-p. The upper part of VB starts about -5.75 eV. The VB near Fermi level is dominated by S-p and also a little contribution by the states of Pb-s and Pb-p. Now the third region is the CB in which the lower part dominated by Pb-p and S-p also has a little contribution from S-s. **For** Pb_8S_8 as shown in Fig. 4.10 (b) Pb-s state has major contribution to lower part of VB this region also due to a little contribution by the states of S-s S-p and Pb-p. VB near Fermi level is dominated by S-p and a little contribution by the states of Pb-s and Pb-p. Additionally, the third region which is the lower part of CB were dominated by Pb-p and S-p, but S-s showed little contribution. **DOS of** $Ga_1Pb_7S_8$ as show in Fig. 4.11 the lower part of VB is due to high contribution from the Pb-s states, but little contributions of S-s S-p and Pb-p. VB near Fermi level is dominated by S-p and little contribution of Ga-s, Ga-p, Pb-s and Pb-p states. As clearly shown the region around Fermi level, especially very closer to Fermi level, the region was falling with the influence of s and p state of Ga and S atoms and the region which is the lower part of CB were dominated by Pb-p Ga-s, Ga-p and S-p but less dominated by contribution from S-s. As the result shown in Fig. 4.12 illustrates, the lower part of $Ga_2Pb_6S_8$ VB is due to high contribution from the Pb-s and a little contribution of S-s S-p and Pb-p, and the upper part of VB is dominated by S-p with little contribution by the states of Ga-s, Ga-p, Pb-s states and Pb-p. The region around Fermi level specially very closer to Fermi level mostly were influenced by s and p state of Ga and S atoms. The lower part of CB is the region near to Fermi level were dominated by Pb-p, Ga-s, Ga-p and S-p

with little contribution from S-s. Again Pb-s state dominates lower part of VB as $Ga_3Pb_5S_8$ DOS result shown in Fig. 4.13 with little contribution of S-s S-p and Pb-p. upper part of VB dominated by S-p and little contribution by the states of Ga-s, Ga-p, Pb-s and Pb-p. The region around Fermi level, especially very closer to Fermi level, were mostly influenced by s and p state of Ga and S atoms. Also, the region which is the lower part of CB were dominated by Pb-p Ga-s, Ga-p and S-p with little contribution from S-s. **Finally, DOS of** $Ga_4Pb_4S_8$ shown in Fig. 4.14 the lower part of VB is due to high contribution from the Pb-s states, but little contribution of S-s S-p and Pb-p. VB near Fermi level is dominated by S-p and little contribution by the states of Ga-s, Ga-p, Pb-s and Pb-p, moreover, the lower part of CB were dominated by Pb-p Ga-s, Ga-p and S-p with little contribution from S-s. **All DOS results of** $Ga_1Pb_7S_8$, $Ga_1Pb_7S_8$ $Ga_1Pb_7S_8$ and $Ga_1Pb_7S_8$ Pb-s state has high contribution in lower part of VB and S-s, S-p and Pb-p states has little contribution. In both VB and CB region near the Fermi level Ga-s, Ga-p Pb-s, Pb-p and S-p were dominated. The Fermi level also shifted to the left this means the result in the band calculation verified again in DOS results.

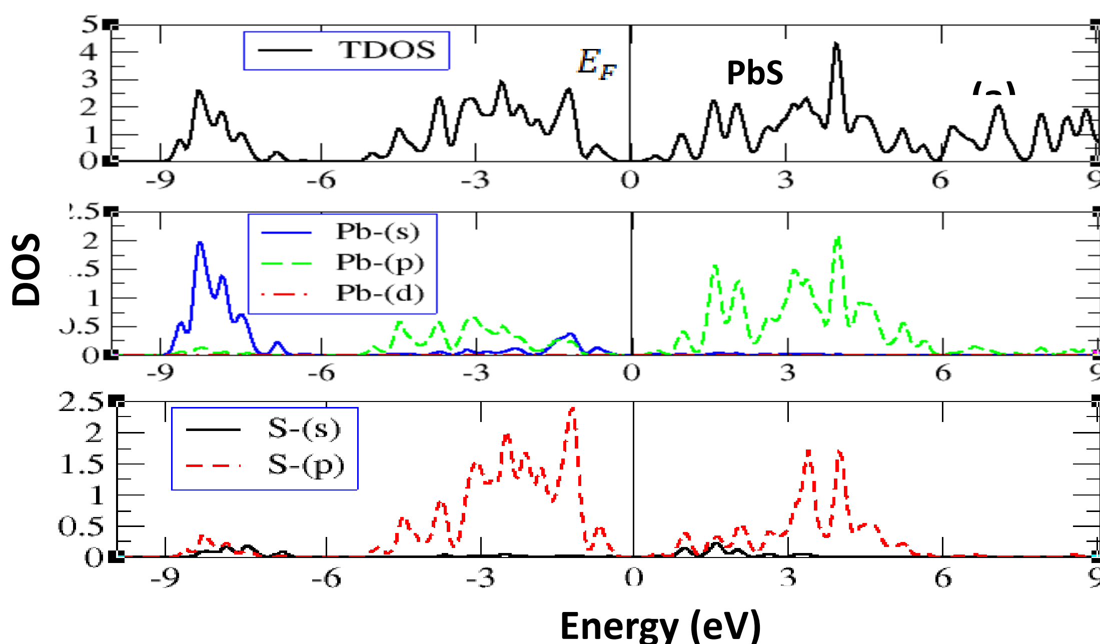

(a)

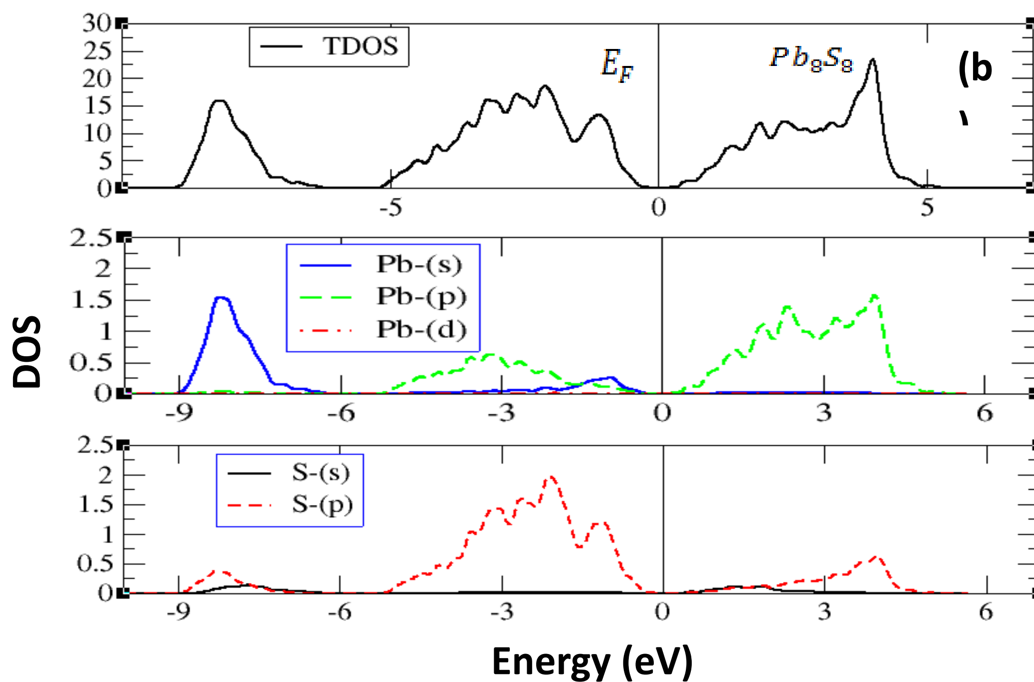

(b)

Figure 4.11: DOS of (a) PbS and (b) Pb_8S_8

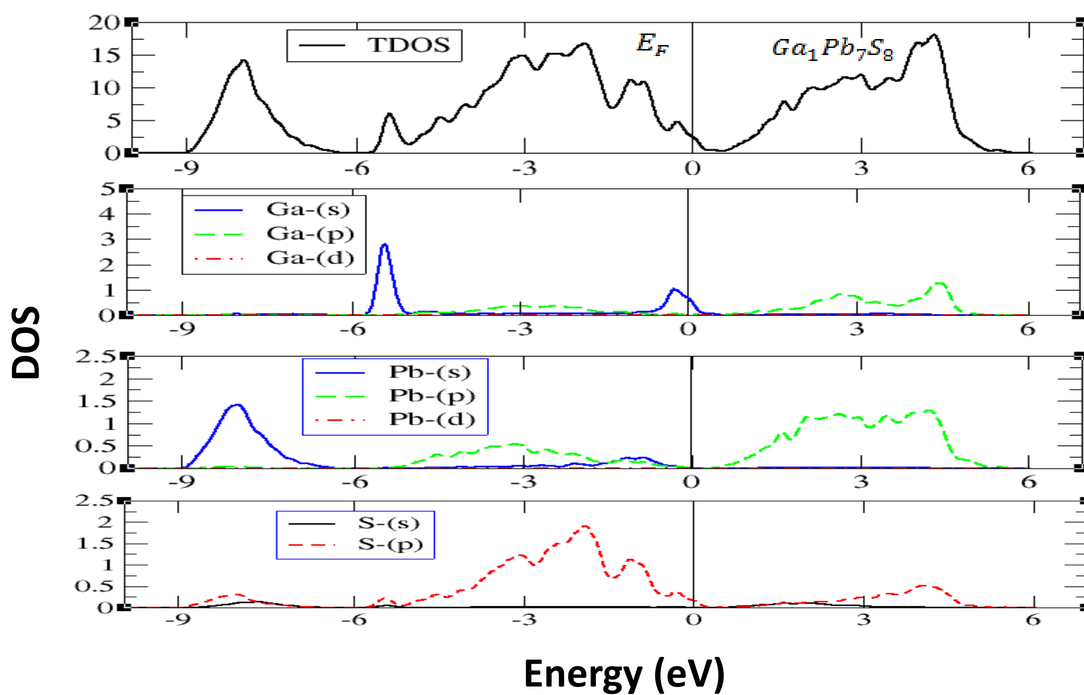

Figure 4.12: DOS of $Ga_1Pb_7S_8$

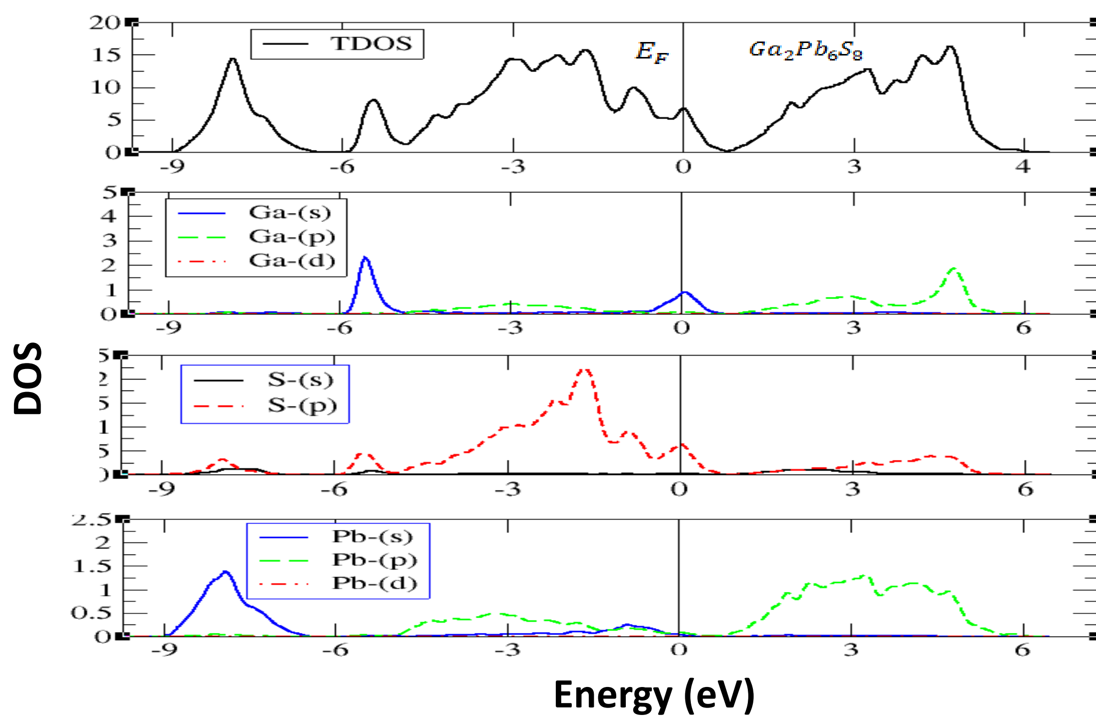

Figure 4.13: DOS of $Ga_2Pb_6S_8$

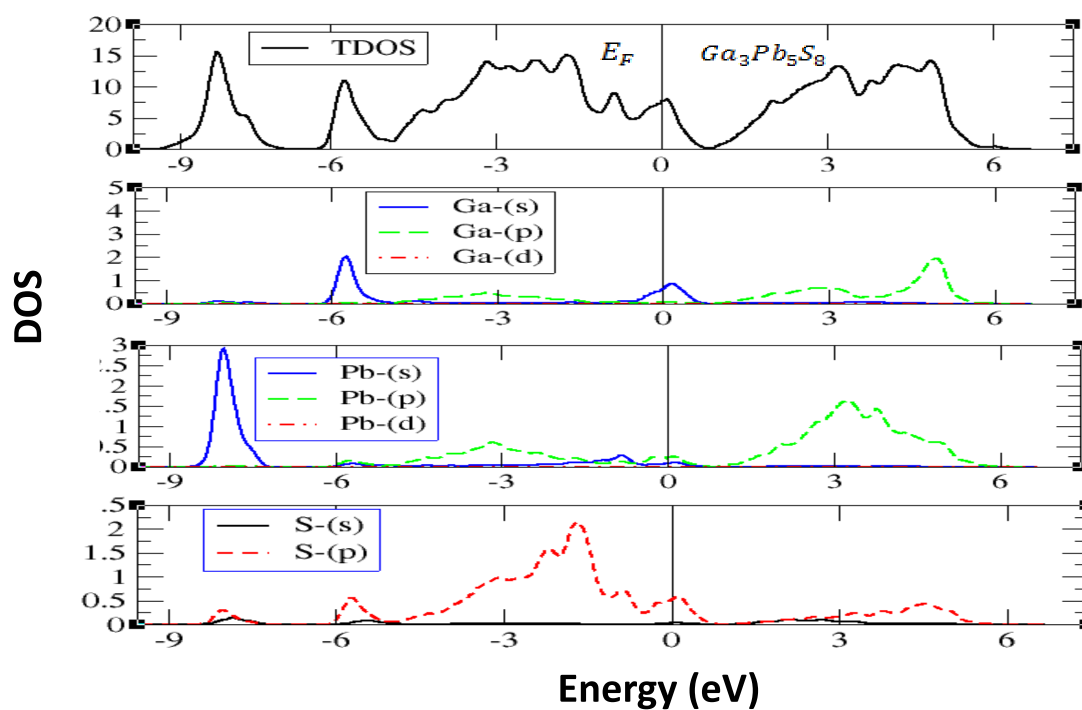

Figure 4.14: DOS of $Ga_3Pb_5S_8$

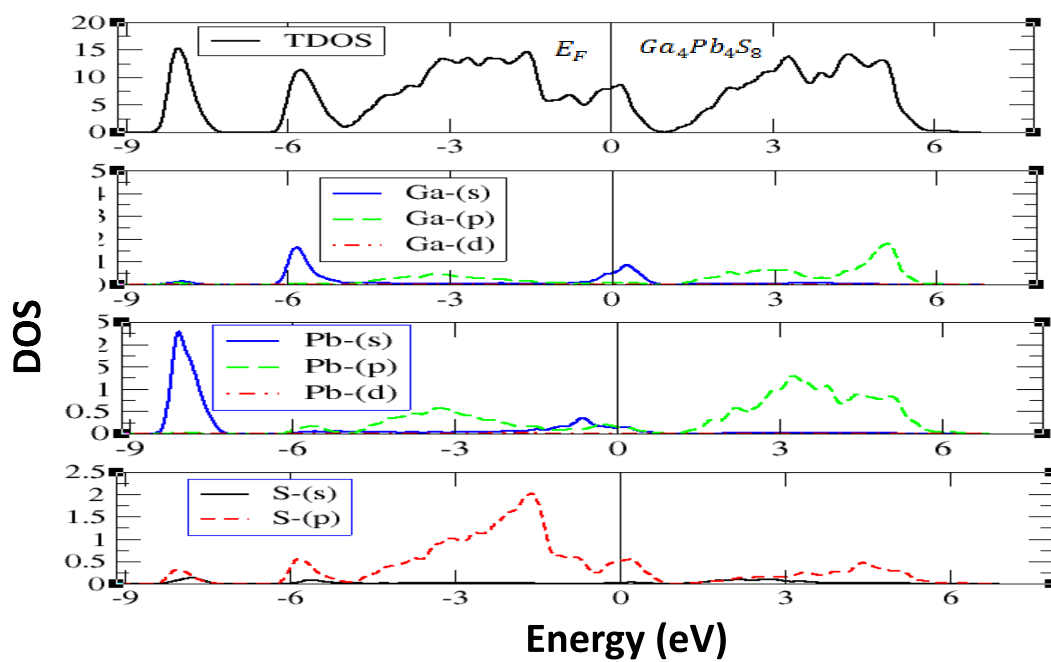

Figure 4.15: DOS of $Ga_4Pb_4S_8$

CHAPTER 5

Conclusion

In the present study, we successfully studied the influence of Ga doping on the structural and optical properties of PbS both experimentally and computationally. The experimental results confirmed that hexamethylenediamine can be used as an alternative complexing agent to synthesis quality Ga doped and undoped PbS. The XRD studies showed that Ga incorporation had a significant influence on the structural parameters of the prepared thin films. The XRD results also verified that there was a slight peak shift towards to the higher 2θ also to the lower values due to the Ga incorporations. The average crystallite also decreased from 56.48 nm to 37.19 nm when gallium dopant concentration increased from 2% to 15%. Furthermore, the DFT calculation was used in the present work and the performance of two pseudopotentials with PBEsol and PBE functionals were tested. The obtained lattice parameter results revealed that PBEsol functional has a better performance with a value of 5.913 Å which is very close to the theoretical result. Similarly, the energy band gap obtain by PBEsol 0.392 eV is very close to the existing experimental value of 0.41 eV than the one obtained by PBE which is 0.498 eV. The electronic property study also confirmed that the band gap increased with Ga concentrations which is consistent with the experimental findings. The occupied number of states of atoms and their individual contributions were simulated on the PDOS calculation. The obtained results revealed that the VB of the bulk PbS is due to the contributions of Pb-s, S-p and Pb-p states while, CB is due to **S-p, S-s and Pb-p states. For Ga doped** Ga**-s, Ga-p,** Pb-s S-s, S-p states contributed for VB formation whereas, CB formed due the contributions from **Ga-p, Pb-p and S-p** states **with a** little input from Ga**-s** state. However, the doping concentrations are different both the experimental and DFT results found in the present study are consistent each other.

References

1. Yu, Peter (2010). Fundamentals of Semiconductors. Berlin: Springer-Verlag. ISBN 978-3-642-00709-5.
2. Donald A. Neamen Univer" Semiconductor Physics and Devices Basic Principles Third Edition: ip of New Mexico
3. Mott, N. (1969)."Observation of Anderson Localization in an Electron Gas". Physical Review.181 (3): 1336.
4. Charles Kittel (1995) Introduction to Solid State Physics, 7th ed. Wiley, ISBN 0-471-11181-3.
5. Md. Atikur Rahman (2014). A Review on Semiconductors Including Applications and Temperature Effects in Semiconductors. American Scientific Research Journal for Engineering, Technology, and Sciences (ASRJETS) Volume 7, No 1, pp 50-70
6. S. Sankar et al (2015) Mg doping effects on the physical properties of lead sulphide thin films. Int.J. ChemTech Res.2014-2015,7(2),pp 980-986.
7. Chidambara Kumar et al (2014). Structural, Optical and Magnetic studies of Mn doped PbS Thin Films by SILAR method. Elixir Thin Film Tech. 76 (2014) 28336-28340
8. Jiabin Huo (2019), Effect of Cr Doping Concentration on the Structural, optical, and Electrical Properties of Lead Sulfide (PbS) Nanofilms, Coatings 2019, 9, 376.doi:10.3390/coatings9060376
9. Y. Gülen (2014), Characteristics of Ba-Doped PbS Thin Films Prepared by the SILAR Method Vol. 126 (2014) ACTA PHYSICA POLONICA A No. 3, DOI: 10.12693/APhysPolA.126.763
10. M. G. Faraj, F. A. I. Chaqmaqchee, H. D. Omar (2017). Structural, morphological and electrical properties of Zn doped PbS thin Films by chemical spray pyrolysis technique, Journal of Optoelectronics and Advanced Materials Vol. 19, Iss. 5-6, pp. 412-416
11. Reshmi Radhakrishnan (2011). The Effect of Ga Doping on the Physical Properties of Lead Sulphide Thin Films, Optics: Phenomena, Materials, Devices, and Characterization. AIP Conf. Proc. 1391, 755-757; doi: 10.1063/1.3643670
12. Hai-Qing Xie et al .(2010). First-principles study on electronic and optical properties of La-doped ZnS.Int. J. Phys. Sci.Vol. 5(17), pp. 2672-2678, 18
13. Heidi D. Nelson et al.(2016) Computational Studies of the Electronic Structures of Copper-Doped CdSe Nanocrystals: Oxidation States, Jahn-Teller Distortions, Vibronic Bandshapes, and Singlet Triplet Splittings. J. Phys. Chem.

14. M. Junaid Iqbal Khan et al. (2018), Effect of Ni concentration on optical properties of rocksalt CdS system (A DFT + U study) International Journal of Modern Physics B Vol. 32. DOI:10.1142/S021797921850280M.

15. Junaid Iqbal Khan et al. (2019). Investigation of optical properties of CdS for various Na concentrations for nonlinear optical applications (A DFT study)

16. S.C. Singhal (2000). "Advances in solid oxide fuel cell technology", Solid State Ionics,135(14),p. 305-313.

17. C. Voisard, U. Wiessen, E. Batawi and R. Kruschwitz, (2002). "High Performance Commercial Solid Oxide Fuel Cells", in Fifth European Solid Oxide Fuel Cell Forum, ed. J. Huijsmans, vol. 1,), European Fuel Cell Forum, Oberrohrdorf, Switzerland, p. 18-25.

18. S.P.S. Badwal, R. Deller, K. Foger, Y. Ramprakash and J.P. Zhang, (1997). Interaction between chromia forming alloy interconnects and air electrode of solid oxide fuel cells. Solid State Ionics,99(3-4), p. 297-310.

19. T. Ishihara, H. Matsuda and Y. Takita, (1994.) Doped LaGaO Perovskite Type Oxide as a New Oxide Ionic Conductor. Journal of the American Chemical Society, 116(9). p.3801-3803.

20. M. Gödickemeier and L.J. Gauckler (1998). Engineering of Solid Oxide Fuel Cells with Ceria-Based Electrolytes, Journal of the Electrochemical Society,145(2), p. 414-421.

21. S.W. Tao, F.W. Poulsen, G.Y. Meng and O.T. Sorensen. (2000). High-temperature stability study of the oxygen-ion conductor La0.9Sr0.1Ga0.8Mg0.2O3-x. Journal of Materials Chemistry, 10(8), p. 1829-1833.

22. S.A. Barnett (1990). A New Solid Oxide Fuel Cell Design Based on Thin Film Electrolytes. Energy,15(1). p. 1-9.

23. G. Hodes. (2002). Chemical solution deposition of semiconductor films, Marcel Dekker, Inc.New York. T. P. Niesen and M. R. De Guire. (2001), J. Electroceramics 6, 169

24. S. M. H. Al-Jawad, F. H.Alioy. (2013). Kinetics of Growth and Structural Characterization of Cd1-X ZnxS Thin Films Synthesized By CBD Method, Eng. & Tech. Journal.,31,505-519.

25. P. Srinivasan, P. Rajesh (2012), Effect of temperature on the structural and optical properties of chemically deposited PbS thin films, Elixir Thin Film Tech., 42, 6206-6208.

26. Anuar Kassim. (2010), Effect of bath temperature on the chemical deposition of PbSe. Kathmandu University Journal of Science, Engineering and Technology Vol_6, No II, pp 126-132.

27. F. G. Hone, F. K. (2016). Ampong, Effect of deposition temperature on the structural, morphological and optical band gap of lead selenide thin films synthesized by chemical bath deposition method, Mater Chem Phys. 183, 320-325.

28. Barote Maqbul A, Ingale Babasaheb D, Tingre Govind D, Yadav Abhijit A,

29. Surywanshi Rangrao V, Masumdar Elahipasha U. (2011) Some Studies on Chemically Deposited n-PbSe Thin Films, Research Journal of Chemical Sciences. 1(9): 37-41.

30. Agrawal P, Sachdeva M, Singh A, Suthar B, Bhargava A. (2013). Influence of bath parameters on the structure and optical properties of CdSe nanocrystalline thin films, AIP Conference Proceedings.1536: 169-170

31. N. H. Sheeba, A. Namitha2, K. M. Ramsiya2, T. M. Ashitha3, R. Suhail. (2021). Effect of Deposition Time on Structural and Optoelectronic Properties of Flower-Like Nanostructured PbS Thin Films. J. Sci. Res. 13 (1), 9-20.

32. Milton Ohring. (1992).The Materials Science of Thin Films-Academic Press

33. R. G. Parr, and W. Yang. (1989). Density-Functional Theory of Atoms and Molecules, OUP. Oxford.

34. P. Hohen urg and W. Kohn (1964), Phys. Rev. 136 B864

35. Kohn, Walter; Sham, Lu Jeu (1965). Self-Consistent Equations Including Exchange and Correlation Effects". Physical Review. 140 (4A): A1133–A1138.Bibcode:1965PhRv..140.1133K .doi:10.1103/PhysRev.140.A1133

36. Parr, Robert G.; Yang, Weitao (1994). Density-Functional Theory of Atoms and Molecules. Oxford University Press. ISBN 978-0-19-509276-9. OCLC 476006840. OL 7387548M

37. E. Fermi Z. Phys. 48 73 (1928); L. H. Thomas, Proc. Camb. Phil. Soc. 23 542 (1927); these articles are reproduced in N. H. March, Self-Consistent Fields in Atoms, Plenum, Oxford, (1975).

38. J. P. Perdew and Y. Wang, Phys. Rev. B 33, 8800, (1986); Ibid. E 34, 7406, (1986)

39. J. P. Perdew (1991), in Electronic Structure of Solids 91, Ed. P. Ziesche and H. Eschrig , Akademie Verlay, Berlin.

40. N. W. Ashcroft and Mermin (1976). Solid State Physics. Saunders College Publishing, Schwerdtfeger, P. (2011), "The Pseudopotential Approximation in Electronic Structure Theory", ChemPhysChem, 12 (17): 3143–3155

41. Simone di Cataldo. (2019) “A quick introduction to Quantum Espresso”.

42. Hone FG, Dejene FB. J Mater (2017). Sci Mater Electron.28:5979-5989.

43. Hone FG, Dejene FB, Echendu OK. (2018). Band gap tailoring of chemically synthesized lead sulfide thin films by in situ Sn doping. Surf Interface Anal. 50:648–656

44. Kumar R, Das R, Gupta M, Ganesan V. (2014). Preparation of nanocrystalline Sb doped PbS thin films and their structural, optical, and electrical characterization. Superlattices Microstruct.75:601-612.

45. Portillo Moreno O, Gutiérrez Pérez R, Palomino Merino R, Chávez Portillo M,

46. Hernández Téllez G, Rosas ER. (2016). Optical and structural properties of PbSIn3+ nanocrystals grown by chemical bath. Thin Solid Films.616:800-807.

47. Rajashree C, Balu AR, Nagarethinam VS. (2016). Influence of Al doping on the structural, morphological and opto-electrical properties of spray deposited lead sulfide thin films. J Mater Sci Mater Electron.27(8):7876-7882

48. Akin N, Ozen Y, Ibrahim Efkere H, Cakmaka M, Ozcelik S. Surf Interface Anal. (2014).47:93-98.

49. S.Thirumavalavan, K.Mani, S.Suresh, (2015) Investigation on structural, optical, morphological and electrical properties of lead sulphide (pbs) thin films. Journal of Ovonic Research Vol. 11, No. 3, May - June, p. 123 – 130.

50. Asghar Khan M, Shah ZA, Khan J, Arafat Y, Hayat S, et al. (2017) Principle Investigation of Structural, Electronics and Chemical Properties of Sn Doped PbX (X=S, Se, Te). J Theor Comput Sci 4: 159. doi:10.4172/2376-130X.100015

51. Zhong-Zhen Luo, Shiqiang Hao, Songting Cai, et al (2019). Enhancement of Thermoelectric Performance for n-Type PbS through Synergy of Gap State and Fermi Level Pinning. J. Am. Chem. Soc., 141, 6403-6412. DOI: 10.1021/jacs.9b01889

52. D. Khokhlov, New York: Taylor and Francis, Lead Chalcogenides (2002): Physics and Applications, ed.

Appendixes

1. JCPDS database number (PbS-005-0592)

Name and formula

Reference code:	00-005-0592
Mineral name:	Galena, syn
Compound name:	Lead Sulfide
PDF index name:	Lead Sulfide
Empirical formula:	PbS
Chemical formula:	PbS

Crystallographic parameters

Crystal system:	Cubic
Space group:	Fm-3m
Space group number:	225
a (Å):	5.9362
b (Å):	5.9362
c (Å):	5.9362
Alpha (°):	90.0000
Beta (°):	90.0000
Gamma (°):	90.0000
Calculated density (g/cm^3):	7.60
Measured density (g/cm^3):	7.57
Volume of cell (10^6 pm^3):	209.18
Z:	4.00
RIR:	-

Subfiles and quality

Subfiles: Alloy, metal or 61ntermetallic
Common Phase
Educational pattern
Forensic
Inorganic

	Mineral
	NBS pattern
Quality:	Indexed (I)

Comments

Color:	Gray metallic
Creation Date:	01/01/1970
Modification Date:	14/01/2012
Additional Patterns:	To replace 00-022-0652 and validated by calculated pattern. See PDF 01-078-1054, 01-078-1055, 01-078-1056, 01-078-1057, 01-078-1058, 01-078-1897 and 01-077-0244
Analysis:	Spectroscopic analysis: <0.01% Cu, Fe, Ag, Al, Mg, Si, Sn and Ca in sample. Color: Gray metallic. General Comments: Opaque mineral optical data on synthetic sample: RR2Re= 43.7, Disp.=16, VHN100=59-65, Color values=.304, .309, 43.7, Ref.: IMA Commission on Ore Microscopy QDF. Sample Source or Locality: Sample from National Lead Company. Temperature of Data Collection: Pattern taken at 299 K. Unit Cell Data Source: Powder Diffraction.

References

Primary reference:	Swanson, Fuyat., *Natl. Bur. Stand. (U. S.), Circ. 539*, **II**, 18, (1953)

Peak list

No.	h	k	l	d [A]	2Theta[deg]	I [%]
1	1	1	1	3.42900	25.964	84.0
2	2	0	0	2.96900	30.075	100.0
3	2	2	0	2.09900	43.059	57.0
4	3	1	1	1.79000	50.978	35.0
5	2	2	2	1.71400	53.413	16.0
6	4	0	0	1.48400	62.540	10.0
7	3	3	1	1.36200	68.883	10.0
8	4	2	0	1.32700	70.969	17.0
9	4	2	2	1.21200	78.923	10.0
10	5	1	1	1.14240	84.797	6.0
11	4	4	0	1.04890	94.511	3.0
12	5	3	1	1.00340	100.294	5.0
13	6	0	0	0.98930	102.271	6.0
14	6	2	0	0.93860	110.308	4.0
15	5	3	3	0.90500	116.676	2.0
16	6	2	2	0.89520	118.741	4.0
17	4	4	4	0.85680	128.065	1.0
18	7	1	1	0.83120	135.862	3.0
19	6	4	0	0.82320	138.696	3.0

Stick Pattern

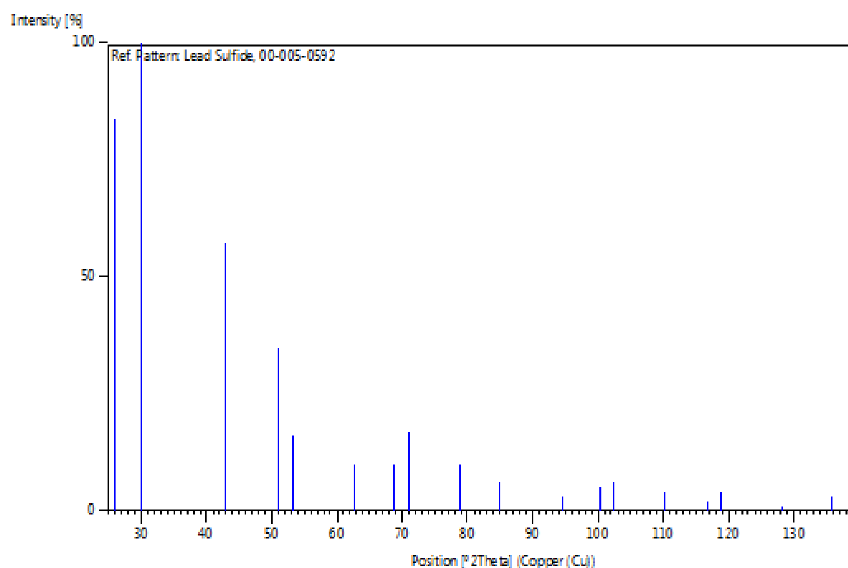

2. QE input files.

Scf input for PbS,

```
&SYSTEM
    a           =  6.00645e+00
    degauss     =  1.00000e-02
    ecutrho     =  4.13717e+02
    ecutwfc     =  4.59686e+01
    ibrav       = 2
    nat         = 2
    ntyp        = 2
    nbnd        = 20
    occupations = "smearing"
    smearing    = "gaussian"
/

&ELECTRONS
    conv_thr          =  1.00000e-06
    electron_maxstep = 200
    mixing_beta       =  7.00000e-01
    startingpot       = "atomic"
    startingwfc       = "atomic+random"
/

K_POINTS {automatic}
 4  4  4  0 0 0

ATOMIC_SPECIES
Pb     207.20000  Pb.pbe-dn-rrkjus_psl.1.0.0.UPF
S       32.06600  S.pbe-nl-rrkjus_psl.1.0.0.UPF

ATOMIC_POSITIONS {angstrom}
Pb      0.000000   0.000000   0.000000
S      -3.003223   3.003223   3.003223
```

Scf for Super cell

```
&SYSTEM
    a            =  1.20129e+01
    degauss      =  1.00000e-02
    ecutrho      =  4.13651e+02
    ecutwfc      =  4.59612e+01
    ibrav        = 2
    nat          = 16
    ntyp         = 2
    nbnd         = 100
    occupations  = "fixed"
    smearing     = "gaussian"
/

&ELECTRONS
    conv_thr          =  1.00000e-06
    electron_maxstep  = 200
    mixing_beta       =  7.00000e-01
    startingpot       = "atomic"
    startingwfc       = "atomic+random"
/

K_POINTS {automatic}
 2  2  2  0 0 0

ATOMIC_SPECIES
Pb    207.20000  Pb.pbesol-dn-rrkjus_psl.1.0.0.UPF
S      32.06600  S.pbesol-nl-rrkjus_psl.1.0.0.UPF

ATOMIC_POSITIONS {angstrom}
Pb      0.000000   0.000000   0.000000
S      -3.003223   3.003223   3.003223
Pb     -3.003225   3.003225   0.000000
S      -6.006448   6.006448   3.003223
Pb      0.000000   3.003225   3.003225
S      -3.003223   6.006448   6.006448
Pb     -3.003225   6.006450   3.003225
S      -6.006448   9.009673   6.006448
Pb     -3.003225   0.000000   3.003225
S      -6.006448   3.003223   6.006448
Pb     -6.006450   3.003225   3.003225
S      -9.009673   6.006448   6.006448
Pb     -3.003225   3.003225   6.006450
S      -6.006448   6.006448   9.009673
Pb     -6.006450   6.006450   6.006450
S      -9.009673   9.009673   9.009673
```

Scf for Ga 12.5% doping

```
&SYSTEM
    a            =  1.1825e+01
    degauss      =  1.00000e-02
    ecutrho      =  4.13651e+02
    ecutwfc      =  4.59612e+01
    ibrav        = 2
    nat          = 16
    ntyp         = 3
    occupations = "smearing"
    smearing     = "gaussian"
/

&ELECTRONS
    conv_thr          =  1.00000e-06
    electron_maxstep = 200
    mixing_beta       =  7.00000e-01
    startingpot       = "atomic"
    startingwfc       = "atomic+random"
/

K_POINTS {automatic}
 2  2  2  0 0 0

ATOMIC_SPECIES
Pb     207.20000  Pb.pbesol-dn-rrkjus_psl.1.0.0.UPF
S       32.06600  S.pbesol-nl-rrkjus_psl.1.0.0.UPF
Ga      69.72300  Ga.pbesol-dnl-rrkjus_psl.1.0.0.UPF

ATOMIC_POSITIONS {angstrom}
Ga       0.000000   0.000000   0.000000
S       -3.003223   3.003223   3.003223
Pb      -3.003225   3.003225   0.000000
S       -6.006448   6.006448   3.003223
Pb       0.000000   3.003225   3.003225
S       -3.003223   6.006448   6.006448
Pb      -3.003225   6.006450   3.003225
S       -6.006448   9.009673   6.006448
Pb      -3.003225   0.000000   3.003225
S       -6.006448   3.003223   6.006448
Pb      -6.006450   3.003225   3.003225
S       -9.009673   6.006448   6.006448
Pb      -3.003225   3.003225   6.006450
S       -6.006448   6.006448   9.009673
Pb      -6.006450   6.006450   6.006450
S       -9.009673   9.009673   9.009673
```

DECLAREATION

ADDIS ABABA UNIVERSITY

COLLEGE OF NATURAL AND COMPUTATIONAL SCIENCES

DEPARTMENT OF PHYSICS

MSc Thesis

Effects of Ga doping on the structural, optical and electronic properties of PbS:

Experimental and computational study

Name of Candidate: Kelemu Teshome Assefa

I the under signed declare that the thesis is my original work and no part of it can be claimed as an intellectual property of anybody else except and my advisors.

Signature: _______________________